AN ABSTRACT OF THE THESIS OF

Chun-Ta Huang for the degree of Master of Science in Electrical & Computer Engineering presented on July 10, 1992.

Title: A Study of Deep Levels of AlGaAs/GaAs Heterojunction Bipolar Transistors

Redacted for Privacy

Abstract approved: _____
John F. Wager

A study of deep levels of the emitter region of a heterojunction bipolar transistor is investigated using deep level transient spectroscopy (DLTS), deep level admittance spectroscopy (DLAS), thermally stimulated capacitance (TSCAP), and capacitance-voltage (C-V) profiling. The DX center, with an activation energy of 0.45 eV, is the only deep level detected. By varying the DLTS rate window and filling pulse widths, DX is found to be comprise of two closely spaced DX centers, denoted DX_1 and DX_2. A positive peak observed in the DLTS spectra is attributed to electron capture, not minority carrier emission, and, thus, is an experimental artifact. Finally, the reduction of current gain (β) at low collector current and the effect of the DX center on the switching characteristics of HBTs are briefly discussed.

A Study of Deep Levels of AlGaAs/GaAs Heterojunction Bipolar Transistors

by

Chun-Ta Huang

A THESIS

submitted to

Oregon State University

in partial fulfillment of
the requirements for the
degree of

Master of Science

Completed July 10, 1992

Commencement June 1993

APPROVED:

Redacted for Privacy

Associate Professor of Electrical and Computer Engineering in charge of major

Redacted for Privacy

Head of Department of Electrical and Computer Engineering

Redacted for Privacy

Dean of Graduate School

Date thesis is presented July 10, 1992

Typed by Chun-Ta Huang

ACKNOWLEDGEMENT

I would like to express my sincere gratitude to my advisor, Professor John F. Wager, for the support, guidance and encouragement he has given me through out this work.

Special thanks to Professor John R. Arthur, Professor Thomas K. Plant, and Professor Gerald A. Smith for serving on my graduate committee and providing useful suggestions.

I would also like to thank Dr. John Ebner and Dr. George Pubanz at Tektronix for providing AlGaAs/GaAs heterojunction bipolar transistors.

Sincere thanks are due to my parents and wife for their constant encouragement and advice.

The financial support provided by the Air Force Office of Scientific Research under contract AFOSR-89-0309 is greatly appreciated.

For my parents and wife

TABLE OF CONTENTS

LIST OF FIGURES

LIST OF TABLES

A Study of Deep Levels of AlGaAs/GaAs Heterojunction Bipolar Transistors

Chapter 1. Introduction

All real semiconductors contain impurities. Some impurities are intentionally introduced as dopant atoms (shallow-level impurities), recombination centers (deep-level impurities) to reduce the device lifetime, or deep-level impurities to increase the substrate resistivity. Many impurities are unintentionally incorporated during crystal growth or device processing. Semiconductor imperfections include foreign impurities (e.g., metals), crystallographic point defects (e.g., vacancies and interstitials), or structural defects (e.g., stacking faults and dislocations).

In semiconductors, when the periodicity of the single crystal is perturbed by foreign atoms or crystal defects, discrete energy levels, E_t, are introduced into the band gap. Such defects are commonly called generation-recombination (G-R) centers or traps. These G-R centers lie deep in the band gap and are known as deep-level impurities. They act as recombination centers when there are excess carriers in the semiconductor and as generation centers when the carrier density is below its equilibrium value, as in the reverse-biased space-charge region (scr) of a p-n junction or Schottky barrier.

For semiconductors such as silicon, germanium, and gallium arsenide, deep levels may arise from metallic impurities like iron, gold, and copper. Deep-level impurities may also result from crystal imperfections, such as dislocations, stacking faults, precipitates, vacancies, and interstitials. Generally, deep levels are undesirable. Occasionally, however, they are intentionally introduced to alter the characteristics of the material or device. Often controlled amounts of deep-level impurities are introduced to reduce the switching time of a device. In semiconductors like GaAs and InP, deep-level impurities are employed to increase the substrate resistivity, rendering it semi-insulating (SI).

There are three different electron and/or hole interaction mechanisms between the deep level, conduction band, and/or valence band [1]; recombination, generation, and trapping, as shown in Fig. 1.1. A recombination event is illustrated by Fig. 1.1(a) followed by (c) and a generation event is (b) followed by (d). The G-R center and both the conduction and valence bands participate in recombination and generation. A third event, which is neither recombination nor generation, is trapping. It is given by Fig. 1.1(a) followed by (b) for an electron or Fig. 1.1(c) followed by (d) for a hole. In either case, a carrier is captured and subsequently emitted back to the band from which it came. Only one of the two bands and the trapping center participate for the trapping event. This investigation is limited to the trapping event.

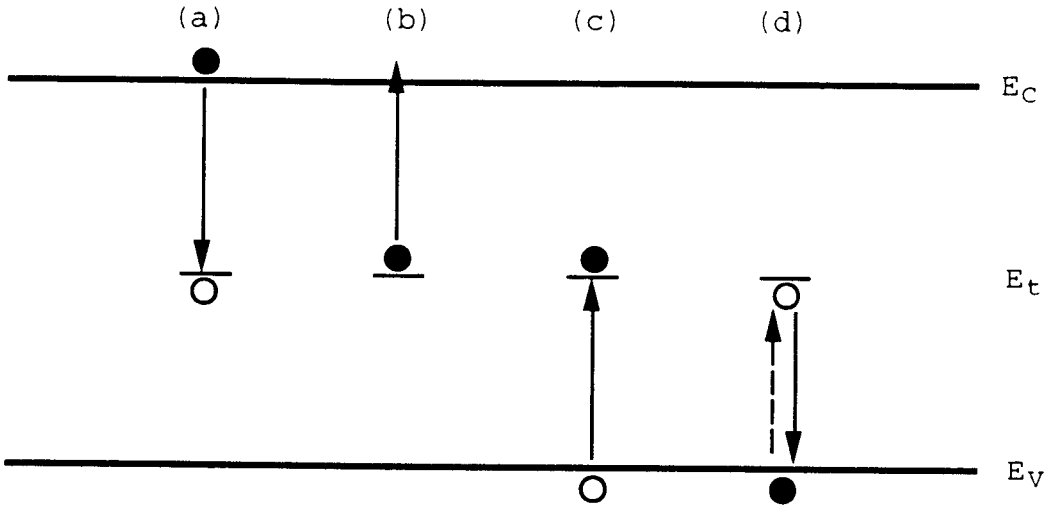

Figure 1.1. Electron energy band diagram for a semiconductor with a deep-level: (a) followed by (c) is a recombination process, (b) followed by (d) is a generation process, and (a) followed by (b) or (c) followed by (d) is a trapping process. The solid and open circles represent electrons and holes, respectively [1].

Deep donor levels, which are often called DX centers, have been observed in many III-V semiconductors. A feature which is rather unique in $Al_xGa_{1-x}As$ ternary crystals grown by liquid phase epitaxy (LPE), molecular beam epitaxy (MBE), and metal-organic chemical vapor deposition (MOCVD) is the appearance of a donor-like deep level which dominates the electrical properties of alloys with $x > 0.22$. This electron trap was originally identified in n-doped LPE crystals [2], and it was found that the trap concentration was proportional to the shallow donor concentration and the defect behaved in a non-effective mass way; that is, this deep level is highly localized in real space, which is different than normal shallow states which are delocalized, effective-mass levels attached to the conduction band minima. The name DX center

has been associated with this defect to account for the fact that this particular deep level is somehow associated with the donor and yet exhibits unusual properties. Since III-V semiconductors have properties which make them attractive for fabricating heterojunction devices such as lasers, light-emitting diodes, and various types of transistors, they have been studied extensively over the last twenty years. DX centers have been extensively studied, not only because of their peculiar properties, but also because an understanding of the physics of this deep level is necessary in order to determine the ultimate usefulness of these materials for heterojunction device structures.

The idea of a heterojunction bipolar transistor (HBT) was proposed by W. Shockley [6] and was later developed by H. Kroemer [7-9]. The basic motivation behind an HBT is the use of a wide-band-gap emitter in the emitter/base junction to provide a higher emitter efficiency; this leads to a higher current gain (β) in HBTs than in homojunction bipolar transistors. The emitter injection efficiency (γ) is also improved by the suppression of base current, which results from a reduction of hole injection from the base into the emitter in the case of an npn HBT. The wide-band-gap emitter removes the doping restrictions in the emitter and base that are necessary for maintaining the current gain in a conventional homojunction bipolar transistor.

The purpose of the work reported in this thesis is to analyze the electrical characteristics of the emitter

junction of Si-doped $Al_{0.25}Ga_{0.75}As$ layers in npn HBTs using C-V profiling, thermally stimulated capacitance (TSCAP), deep level admittance spectroscopy (DLAS), and deep level transient spectroscopy (DLTS) techniques. The effect of DX centers on the performance of HBTs is also investigated.

A review of the literature of the DX center in AlGaAs is presented in Chapter 2 along with a discussion of HBT and HEMT instabilities. Experimental procedures and methods are described in Chapter 3. Subsequently, the experimental results and a discussion of the DX center in AlGaAs HBTs are included in Chapter 4. Finally, Chapter 5 presents conclusions and recommendation for future research.

Chapter 2. Literature Review

2.1. The DX Center in Si-doped AlxGa1-xAs

DX centers, deep levels associated with donors in III-V semiconductors, have been extensively studied and have been reviewed by Lang [20], Mooney [21], Bhattacharya [22], and Bourgoin [23].

The DX center was named by Lang *et al.* [2,24] who suggested that the deep donor level is a complex composed of a substitutional donor atom (D) and an unknown lattice defect (X), possibly an As vacancy. The two primary properties of the DX center in n-type $Al_xGa_{1-x}As$ when $x > 0.22$, are persistent photoconductivity (PPC) [5,25-31] and a large Franck-Condon shift [2,24]. In n-type $Al_xGa_{1-x}As$, PPC occurs at temperatures below 100 °K. When n-type $Al_xGa_{1-x}As$ is exposed to light with energy above band gap, photogenerated carriers are generated and contribute to a significant increase in conductivity; this is the usual situation for photoexcitation of semiconductors. When light is removed, however, the photogenerated carriers persist in the conduction band for hours or even days, depending on the ambient temperature. A large Franck-Condon shift is due to a large difference in the energies of optical and thermal electron emission from the DX state to the conduction band; that is, the photoionization threshold (Ehv) is much larger than the thermal ionization depth (Ee) as shown in Fig. 2.1(a).

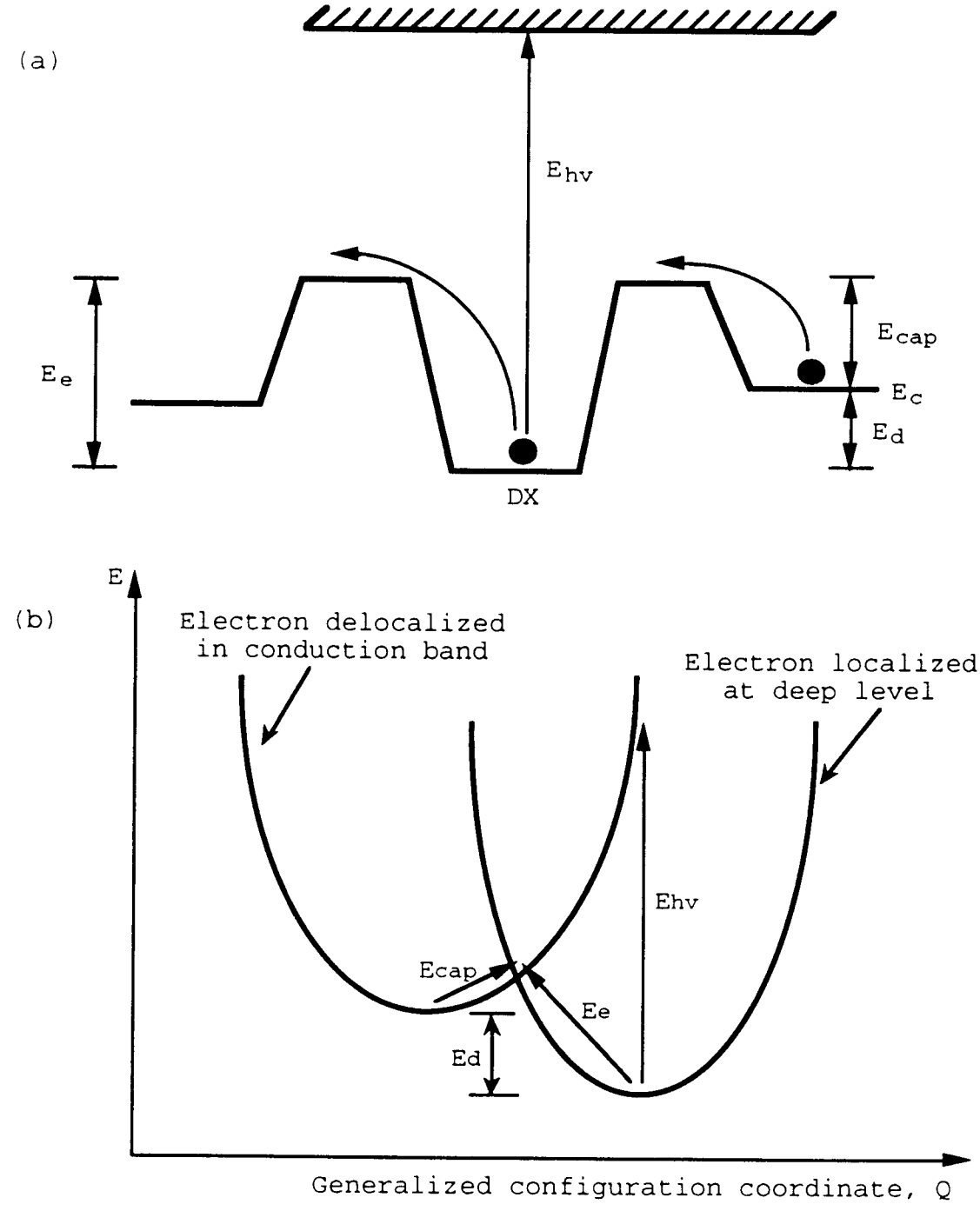

Figure 2.1. (a) A distorted AlxGa1-xAs conduction band relating the PPC effect and large differences in optical (Ehv) and thermal emission (Ee) energies and (b) a configuration coordinate diagram corresponding to (a) [2,24].

In 1977, Lang *et al.*[2,24] suggested that electron capture and emission from DX occurs as a multiphonon process and, hence, that there is a large relaxation of the crystal lattice causing PPC. To account for the large lattice relaxation (LLR), Lang *et al.* proposed the donor-As vacancy model for the DX center. Figures 2.1(a) and 2.1(b) show that a distorted conduction band representation of the DX center and a corresponding generalized configuration coordinate diagram, respectively [2,24]. In these diagrams, four energies are used to characterize the DX center as follows:

1) Ee = thermal emission activation energy,
2) Ecap = capture activation energy (or, capture barrier for an electron),
3) Ed = binding energy, and
4) Ehv = optical emission energy (or, photoionization energy).

The values of these four energies relating to the DX center for various donor-atom AlGaAs are listed in Table 2.1 [21].

Donor species	E_e (eV) (DLTS)	E_{cap} (eV)	E_d (eV) (Hall)	E_e-E_{cap} (eV)	E_{hv} (eV)
Group VI					
S	0.28	-	0.150	-	-
Se	0.28	0.14	0.18	0.14	0.85
Te	0.28	0.14	0.177,0.186	0.14	0.85
Group IV					
Si	0.43	0.21	0.175-0.205	0.22	1.25,1.45
Ge	0.33	-	-	-	-
Sn	0.19,0.21	0.02	0.172,0.201	0.17,0.19	1.11

Table 2.1. Four different energy values related to DX centers for various donor species [21].

The thermal emission activation energy (Ee) of Si-doped AlGaAs for an electron from the DX level to the conduction band, measured by constant capacitance DLTS, is independent of the alloy composition and doping concentration [32-34], as shown in Fig. 2.2 [32]. Also, it is independent of applied hydrostatic pressure for Si-doped AlGaAs [35]. Values of the thermal emission energy of the DX center for different donor species are listed in Table 2.1. The thermal emission energy is much larger than the binding energy indicating that the capture cross section (σ_c) is also temperature dependent.

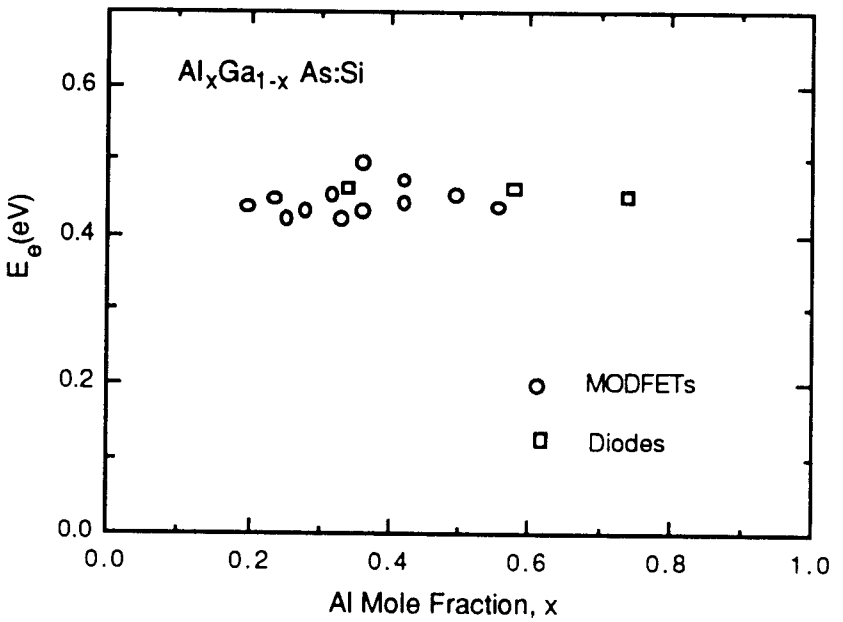

Figure 2.2. Thermal emission energy of the DX center in Si-doped AlGaAs [32].

The capture activation energy (Ecap), which is related to the PPC effect at low temperature, is shown as a function of the alloy composition for Si-doped AlGaAs in Fig. 2.3. The

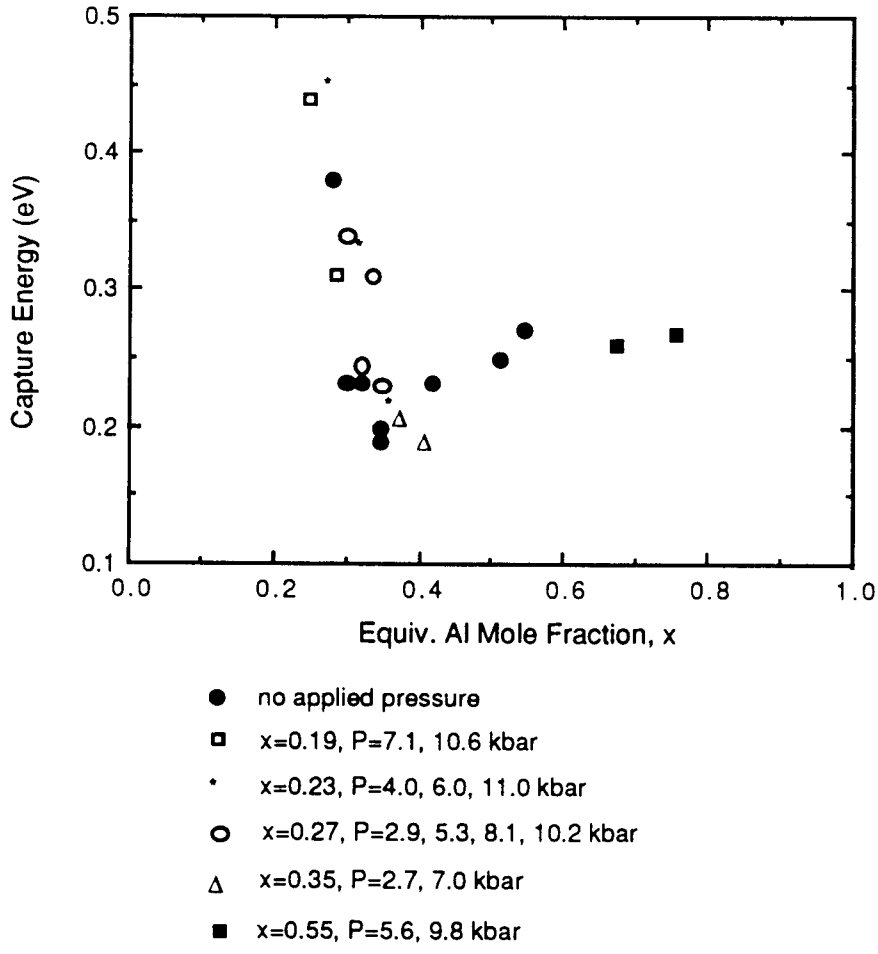

Figure 2.3. The capture activation energy of the DX center is a function of composition and applied pressure [34].

capture barrier for an electron has a minimum value of about 0.2 eV at approximately x = 0.35, near the composition at which AlGaAs goes from direct to an indirect gap semiconductor. However, when hydrostatic pressure is applied, the variation in E_{cap} is due to changes in the band structure. Mooney *et al.* observed that the capture activation energy is a property of the DX center, and not of the heterojunction structure [32]. Thus, the constant emission energy, the variation of the capture energy with the band structure, and

the dependence of the capture rate on the quasi-Fermi level strongly suggest that capture occurs via an intermediate state which is resonant with the conduction band lying at a nearly constant energy above the deep level. While the states of the L valley are an obvious choice for this level, there is no proof that the L-valley states play a special role in the capture process. Capture activation energy values of the DX center for the various donor atoms are also listed in Table 2.1.

The binding energy (Ed), which determines the equilibrium concentration of ionized donors in Si-doped AlGaAs, is assessed from temperature-dependent Hall-effect measurements for different Al compositions [25,36-39]. In Fig. 2.4 [21], when $x < 0.22$, the DX level lies above both the conduction band minima and the effective-mass-like shallow level (which is the hydrogenic level in Fig. 2.3), and may be considered to be a so-called resonant state [40-43]. When $x > 0.22$ up to 0.40, the binding energy increases as x is increased. Beyond the crossover from direct to indirect band gap the DX center moves closer to the bottom of the conduction band. The correlation between binding energy and the band structure is independent of the donor species, and is also observed when the band structure is modified by hydrostatic pressure [34,44]. The values of the DX center binding energies (Ed) for various donor species are also listed in Table 2.1.

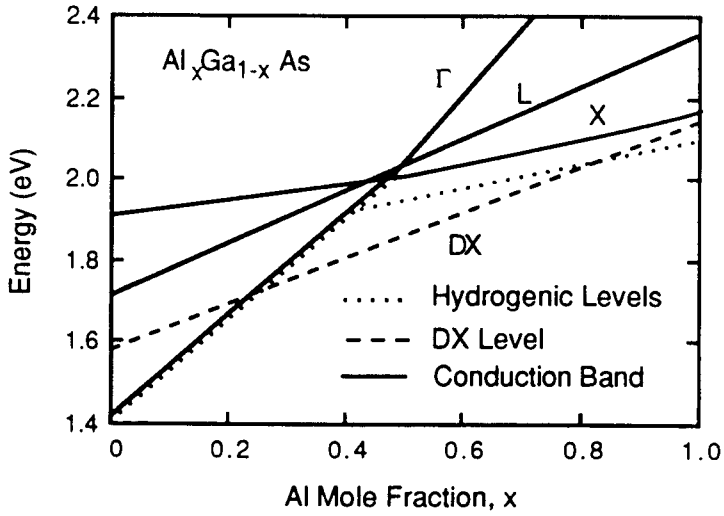

Figure 2.4. Energies of three conduction band minima, hydrogenic levels, and the DX level as a function of the composition of AlGaAs [21].

The optical emission energy (Ehv), which contributes the evidence for the LLR model, is one of the distinctive optical properties of the AlGaAs DX center. The lattice relaxation energy, which is the difference between the optical emission and thermal emission energies, is determined by measuring the energy dependence of the photoionization cross section, σ_n^*. As does the thermal emission energy, the optical emission energy depends on the dopant species [45], as listed in Table 2.1. The large difference between the photoionization energy and the binding energy as well as the temperature dependence of σ_n^* are in agreement with the model for multiphonon capture and emission. The measurements of σ_n^* in Si-doped AlGaAs show little dependence of the photoionization cross section on Al composition, as well as a large photoionization energy and temperature dependence in excellent agreement with the LLR model.

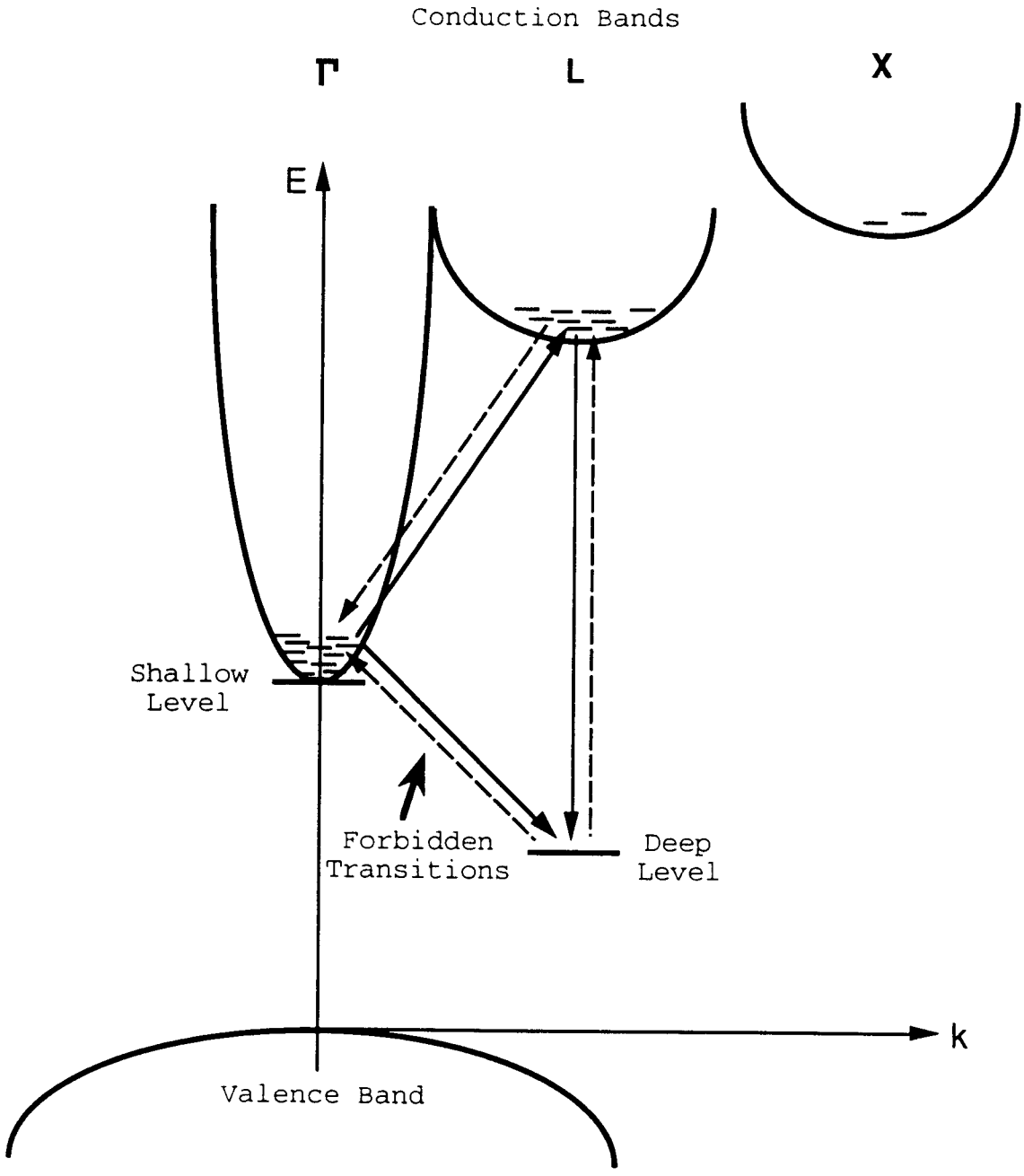

Figure 2.5. A configuration coordinate diagram of the direct-band-gap AlxGa1-xAs. The solid and dashed arrows represent the various possibilities for electron capture and emission by the deep level, respectively [47].

In 1982, Saxena [47] proposed a more explicit multiphonon model using the configuration-coordinate (CC) diagram as, shown in Fig. 2.5, to explain PPC. He suggested that in direct-band-gap alloys, upon photoexcitation at low temperatures, the electrons are emitted from the deep impurity level, to the L band or L minima, and then scattered into the Γ minimum. As shown in Fig. 2.5, after removing the light source, due to the indirect nature of the transitions involved between the Γ minimum and the deep states, the electrons in the Γ minimum are prohibited from either recombining into the deep states or being scattered back to the L minima. Thus, the PPC effect occurs at low temperature. Upon increasing the temperature, however, the electrons are transferred from the Γ minimum to the L minima, and from there they can recombine into the deep states. Supporting evidence that the deep level in AlGaAs is attached to L-conduction-band minimum was presented by Calleja *et al.* [35] in 1988. It was also observed that the DX center lies about 160 meV below the L minimum of the conduction band [36], as shown in Fig. 2.4 [21].

In 1985, PPC effects of Si-doped AlGaAs subjected to hydrostatic pressure were observed by Mizuta *et al.* [49]. Also, a shallow-deep transition in GaAs, occurring at pressures of about 20 ~ 30 kbar, with the pressure for inducing the transition decreasing with increasing Al content [44,47,49-51] was observed. Pressure experiments have been crucial in demonstrating that the shallow-deep transition is

associated with the donor atom itself and that an association of the donor with other defects such as an As vacancy to produce the DX center is unlikely.

In 1988, Chadi and Chang [55,56] proposed that the properties of the DX level in n-type AlGaAs can be accounted for by a negative U center. U is the Hubbard correlation energy and it is negative when capture of a second electron decreases, rather than increases, the energy of a deep level. This happens when the energy due to the repulsion of the two electrons is offset by the energy due to relaxation of the crystal lattice. Thus, this model requires a LLR of the DX center. This LLR is concomitant with electron pairing [57], resulting in a two-electron DX^- ground state with a negative Hubbard correlation energy U:

$$2d^\cdot \text{ ---> } d^+ + DX^-$$

where $d^\cdot$ and d^+ represent neutral and ionized substitutional donors, respectively. DX^- denotes a highly localized and negatively charged center. In an alternative substitutional-donor model [58], the DX center is an isolated substitutional donor with a deep, relaxed ground state and a shallow, unrelaxed metastable state. However, theoretical calculations [59] indicated that such an isolated substitutional donor occupied with only one electron should not be metastable. This was resolved by the negative-U model of the DX center. The negative-U model also accounts for the presence of the DX

center in GaAs under hydrostatic pressure. The model is consistent with all of the available experimental data with the exception of the magnetic susceptibility measurements, which indicated that the DX center is a paramagnetic donor with one unpaired electron [60].

2.2. Heterojunction Bipolar Transistors (HBTs)

In 1951,the idea of an HBT was proposed by W. Shockley [6] and was later developed by H. Kroemer [7-9]. In the 1980's, there has been a rapid growth in the number of publications on III-V HBTs, particularly for the AlGaAs/GaAs materials system. Until the late 1970's, the development of bipolar transistors in III-V materials was not pursued because of the disappointing performance that had been obtained in previous studies. A renewed interest in these devices was stimulated by the development, in the 1970's, of high-quality GaAs material and processes such as ion implantation and epitaxial growth of heterojunctions. Most of the work in the 1970's concentrated on heterojunction phototransistors, but HBTs have demonstrated, since about 1982, the potential for high speed performance superior to silicon bipolar transistors. Improved performance has been demonstrated in ring oscillators, comparators, dividers, and gate arrays, and integration with laser diodes and LEDs has been achieved. There is also recent interest in the use of HBTs as microwave amplifiers and oscillators.

In the HBT with a wide band gap emitter, the electron barrier is smaller than the hole barrier, resulting in preferential injection of electrons across the emitter junction. Thus, the emitter injection efficiency (γ) is increased without strict requirements on doping. Since carrier injection varies exponentially with the barrier height, even a small difference in a barrier can make a very large difference in the injection of electrons or holes into the emitter junction. Neglecting differences in carrier mobilities and other effects, the dependence of carrier injection across the emitter can be approximated as

$$\frac{I_n}{I_p} \propto \frac{N_{nE}}{N_{pB}} e^{\Delta E_g/KT} \quad . \tag{1.1}$$

In this expression, the ratio of electron current, I_n, to hole current, I_p, crossing the emitter junction is proportional to the ratio of the doping in the emitter, N_{nE}, and the base, N_{pB}. In a homojunction bipolar transistor this doping ratio is all there is to work with in designing a useful emitter junction. However, in an HBT there is an additional factor in which the band gap difference, ΔE_g, between the wide-band-gap emitter and the narrow-band-gap base appears in an exponential factor. As a result, a relatively small value of ΔE_g in the exponential can dominate eqn.(1.1). This allows one to choose the doping such that a lower base resistance and emitter junction capacitance can be

obtained without sacrificing current gain. In particular, the base can be heavily doped to reduce the base resistance and the emitter lightly doped to reduce junction capacitance. Therefore, HBTs offer the following general advantages: first, the base resistance can be reduced by higher base doping, and second, the emitter capacitance can be minimized by lower emitter doping.

Other advantages of HBTs over homojunction (Si) bipolar transistors are associated with the superior electron transport properties of III-V semiconductors. Electron mobility plays an important role in the intrinsic device performance; higher electron mobility provides a shorter base transit time, which results in faster transistor operation. The AlGaAs alloy system, that is useful for both high speed and optoelectronic applications, has a high electron mobility for the direct band gap alloys. The high electron velocity, associated with the overshoot phenomenon in these materials, also may be beneficial for transit time reduction. The electron mobility of GaAs is about ten times higher than that of Si at a doping density of ~ 10^{-18} cm^{-3}. Also, the cutoff frequency for GaAs HBTs is expected to be over 100 GHz.

Earlier attempts at HBT fabrication were made with heterojunctions constructed, in the 1960's [10-12], of Ge and/or binary semiconductors, such as Ge/GaAs, Ge/ZnSe, or ZnSe/GaAs. The interface quality of these junctions was not satisfactory. In the 1970's, LPE growth of III-V semiconductors was applied to HBT fabrication and high

current gain was achieved experimentally [13-14]. However, epitaxial layer thickness and doping control in LPE-grown HBTs was not sufficient for high frequency operation.

More recently, the development of new epitaxial growth techniques such as MBE and MOCVD has enabled fabrication of HBT epilayers suitable for high-frequency and high-speed devices. Using these techniques, very high quality HBT epilayer structures have been grown with a dimensional controllability below 100 Å. Also, it is very important that heavy p-type doping of the GaAs base, up to concentrations of around 10^{20} cm^{-3}, can be achieved using Be.

Microwave characteristics of AlGaAs/GaAs HBTs fabricated by MBE were first reported around 1982 [15-16]. A current gain cutoff frequency of over 20 GHz has been reported [17-18]. Application of HBTs to digital circuits is also attractive, because HBTs are superior in their high cutoff frequency due to the material properties of III-V semiconductors and because of the excellent threshold control that is common to bipolar transistors. In 1983, for example, the first emitter coupled logic (ECL) circuit using AlGaAs/GaAs HBTs was reported [19].

The influence of DX centers on characteristics of modulation-doped field-effect transistors (MODFETs) is examined by Nathan *et al.* [69] in 1985. They found the C-V curves for a MODFET shows the threshold voltage shift at low temperature. In 1986, Kastalsky *et al.* [70] found that another deleterious effect of the DX center in MODFETs is the

so-called collapse of the device current-voltage curves at 77 °K in the dark which is caused by the trapping of hot electrons at DX centers. In 1989, Thomasian *et al.* [71] found the so-called kink effect; a sudden rise in the drain current due to the tunneling of trapped electrons from AlGaAs near the AlGaAs/GaAs interface back into the bulk n-AlGaAs layer. In contrast to the MODFET, the effect of the DX center on the performance of HBTs has received little attention.

Chapter 3. Experimental Methods

3.1. Deep Level Transient Spectroscopy

Deep level transient spectroscopy (DLTS) is a high-frequency (1 MHz range) capacitance transient thermal scanning method useful for characterizing deep levels in semiconductors [61,62].

DLTS consists of the following :

(1) Apply a d.c. reverse bias to increase the width of the space charge region of a p-n junction, Schottky barrier, or other junction device. (2) Apply a voltage pulse, which momentarily reduces the reverse bias, or drives the junction into forward bias, such that deep-level traps are filled by electrons or holes. (3) Remove the pulse and monitor the transient response by measuring capacitance(C), conductance(G), or current(I) as a function of time. This transient is due to thermal emission from deep levels. (4) Perform a thermal scan by monitoring the transient response as a function of temperature over a wide range of temperature. In practice, the signal-to-noise ratio is improved by holding the temperature constant, acquiring the transient multiple times, and signal averaging the acquired transients. Obviously, there is a trade-off between signal-to-noise and data acquisition time. (5) The acquired DLTS data consist of a set of signal averaged transients where each transient corresponds to a specific temperature.

The DLTS data are processed after the data are completely acquired. The first step in the evaluation of the DLTS data is to define a rate window. This amounts to choosing two sampling times t_1 and t_2, as illustrated in Fig. 3.1. Note that at high and low temperatures the DLTS signal, $C(t_1) - C(t_2)$, is equal to zero; at low temperature when the thermal emission rate, e, is approximately equal to zero and at high temperature e is large and the transient is already finished prior to the onset of rate window. Figure 3.1 shows the definition of the filling pulse width and the rate window width.

Assuming that the transients are exponential, the emission rate of a particular trap, corresponding to the maximum of the DLTS peak, is as follows :

$$e^{-1} = \tau_{max} = (t_1 - t_2) \left[\ln \left(\frac{t_1}{t_2} \right) \right]^{-1} . \qquad (3.1)$$

The DLTS method still works for non-exponential transients but care must be taken in obtaining absolute trap parameters from the data. Thus, equation (3.1) above is only valid for exponential transients.

From the DLTS spectra, illustrated in Fig. 3.2, we observe the presence of each trap as indicated by a positive or negative peak on a flat baseline plotted as a function of temperature. The heights of these peaks are proportional to their respective trap concentrations, the sign of each peak

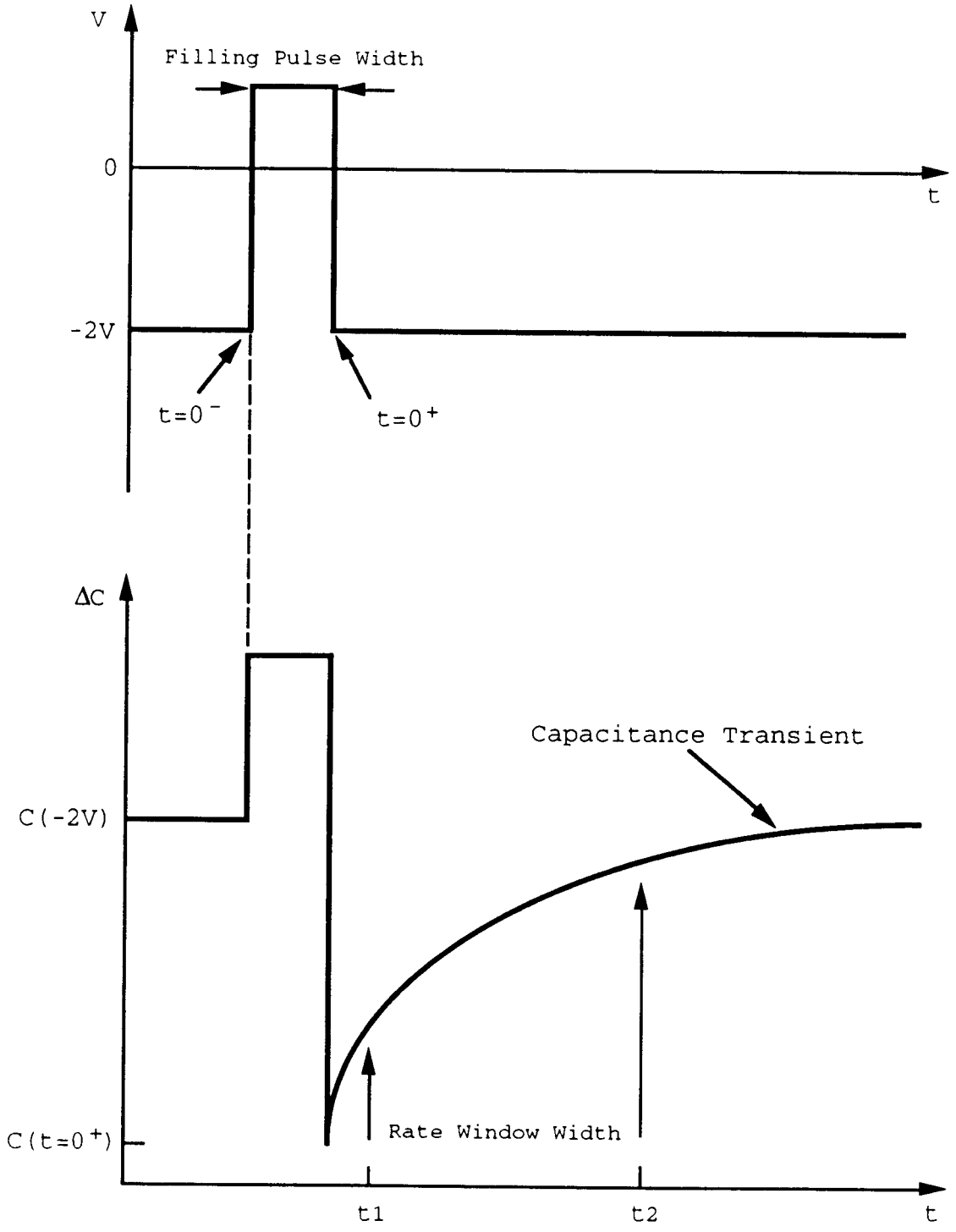

Figure 3.1. Capacitance transients are measured at time t1 and t2 following a filling pulse.

indicates whether it is due to a majority or minority carrier trap (positive peaks corresponds to minority traps and negative peaks to majority traps), and the positions of the peaks are simply and uniquely determined by the rate windows and the thermal emission properties of the respective traps.

There are three options for setting rate windows : (1) fix t_1, vary t_2; (2) fix t_2, vary t_1; and (3) fix the $(\frac{t_1}{t_2})$ ratio, vary both t_1 and t_2. The last alternative, (3), is the one chosen herein because the peaks shift more or less rigidly without significantly changing their shape as the rate window is varied. If method (1) is used and t_1 is fixed while t_2 is varied, the peaks change considerably in both size and shape with the low-temperature side shifting as t_2 is varied, while the high-temperature side moves very little. Method (2) produces exactly the opposite result with the high-temperature side shifting.

An Arrhenius plot is then generated by plotting $\ln(T^2\tau_{max})$ as a function of inverse temperature, as indicated in Fig. 3.3. T^2 arises from the thermal velocity (V_{th}) and the effective density of states (N_c). Thus, by choosing various rate windows and constructing an Arrhenius curve, the activation energy (E_a, eV) can be obtained directly from the slope, and the capture cross section (σ, cm^2) from the intercept as shown in eqns. (2) and (3):

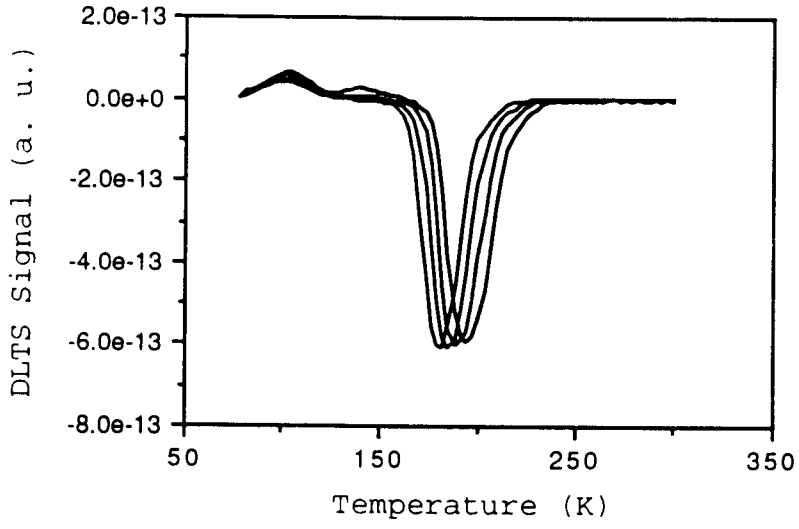

Figure 3.2. DLTS spectra with four different rate windows.

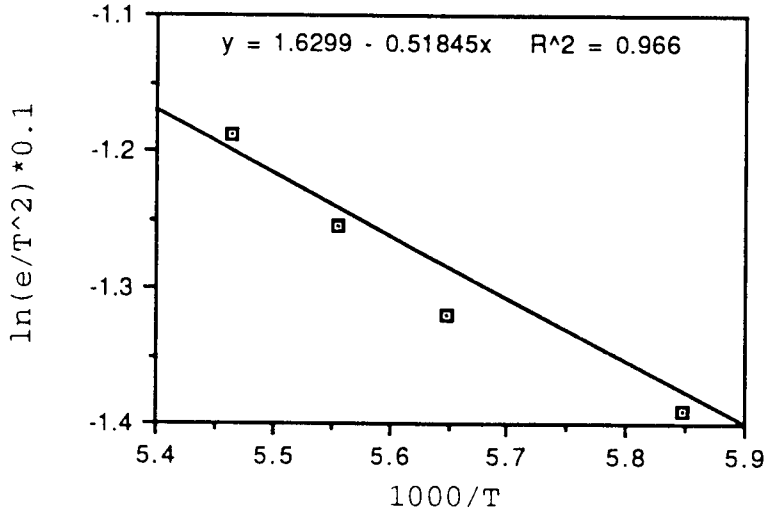

Figure 3.3. From this Arrhenius plot, capture cross section (σ) and the the activation energy (E_a) can be evaluated from the intercept on the y axis and the slope of the line, respectively.

$$e = \frac{1}{\tau_e} = \sigma V_{th} N_c \exp\left(\frac{-E_a}{KT}\right) \qquad (3.2)$$

where, e = thermal emission rate (sec^{-1}), σ = capture cross section (cm^2), V_{th} = thermal velocity (cm/sec), N_c = effective density of states of the conduction band, E_a = activation energy (eV), and K = Boltzmann's constant.Taking the logarithm of eqn. (3.2) yields,

$$\ln e = \left(\frac{-E_a}{K}\right)\left(\frac{1}{T}\right) + \ln\left(\sigma V_{th} N_c\right). \qquad (3.3)$$

Also, trap concentration (N_t, cm^{-3}) can be obtained from the capacitance change due to the voltage pulse at t = 0 ($\Delta C(0)$) as shown below in the following equation,

$$N_t = 2\left(\frac{\Delta C(0)}{C}\right)(N_d - N_a) \qquad (3.4)$$

where, C = the capacitance of the diode under quiescent reverse-biased conditions and $N_d - N_a$ = the net donor concentration on the n side of the junction where the trap is observed. The capture rate (c) of the trap level is given by

$$c = \sigma V_{th} n \qquad (3.5)$$

where n is the doping concentration (cm^{-3}).

Two additional issues need to be mentioned. First, there is an alternative method for more accurately estimating the capture cross section by varying the filling pulse duration. Second, the reasons for observing non-exponential traps are: (1) large trap densities ($N_t \geq 0.1N_{shallow\ dopants}$); (2) the emission rate depends on the magnitude of the electric field due to barrier lowering (Poole-Frenkel effect) or tunneling (field emission) from the trap; (3) the existence of a non-abrupt transition width between the space charge region and the quasi-neutral region.

The DLTS measurement system, as shown in Fig. 3.4, consists of the following components: (1) variable temperature cryostat (35 'K ~ 370 'K), (2) vacuum pump (TRIVAC model D2A), (3) compressor module (model HC-4), (4) programmable temperature controller (R. G. Hansen & Associates Series 8000), (5) HP 9000 series 236 and HP 9133 computers, (6) HP 16083A pulse bias noise clipper, (7) HP 3457A multimeter, (8) HP 8112A pulse generator 50 MHz, (9) HP 6205C Dual d.c. power supply, and (10) HP 4280A 1MHz C meter/C-V plotter.

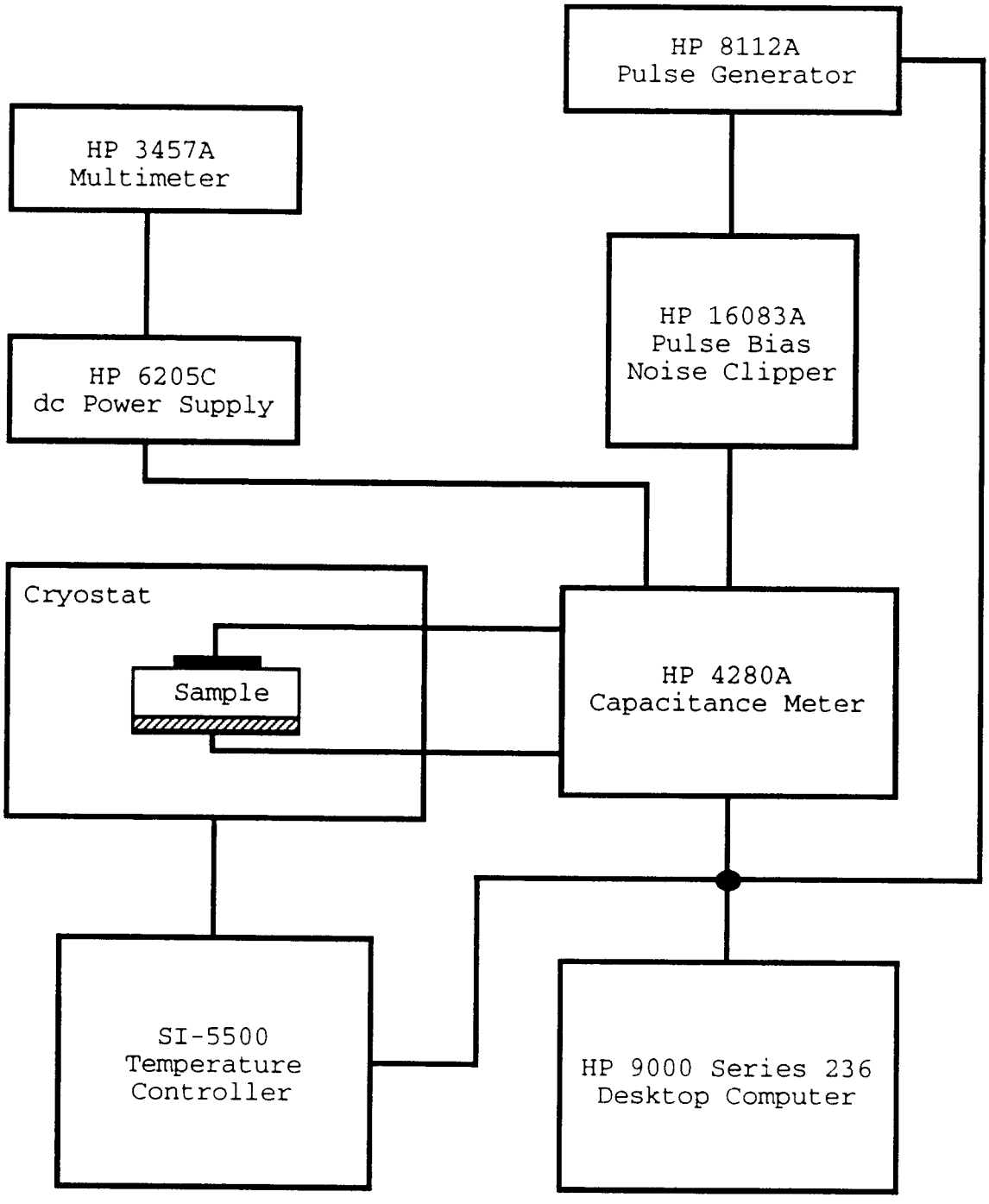

Figure 3.4. Schematic setup for DLTS measurements.

3.2. Deep Level Admittance Spectroscopy

The influence of deep levels on the impedance of a semiconductor device has been recognized for a long time and this effect has been suggested as a way to accomplish deep level analysis. The corresponding method has been described by D. L. Losee and is referred to as admittance spectroscopy [63].

Deep level admittance spectroscopy (DLAS) is a powerful characterization technique for measuring the capacitance (C) and conductance (G) of the junction admittance at several (discrete) frequencies as a function of temperature, which provides a spectroscopy of defect levels (principally, majority-carrier traps).

DLAS basically consists of the following : (1) apply a small ac voltage (about 30 mV) to a Schottky barrier (or, p-n junction) diode. The quasi-Fermi level sweeps through the various defect energy levels, which produces an oscillation in the charge density distribution. The magnitude of the charge density oscillation, $\delta\rho$, is a function of distance from the metal electrode. $\delta\rho$ is peaked roughly at each point where the Fermi level passes through a trap level, provided that the level responds to the test frequency. (2) For a planar junction, the capacitance of the diode is,

$$C = \frac{\varepsilon A}{x_{cg}} \tag{3.6}$$

where, C = capacitance, ε = low-frequency dielectric constant, A = area, x_{cg}= centroid of the $\delta\rho$ distribution. Thus, if the frequency of δV (the applied a.c. signal) or the temperature of the junction changes so that one of the levels cannot respond, then there will be a corresponding shift in x_{cg} and hence a change in C. (3) At intermediate temperatures the change, $\delta\rho_k$, for, say, the kth level, is finite but lags δV, thus producing a real component, or loss, in the admittance. (4) Finally, the conductance (G) versus temperature (T), as shown in Fig. 3.5, and the capacitance (C) versus temperature (T), plots actually constitute the admittance spectroscopy data.

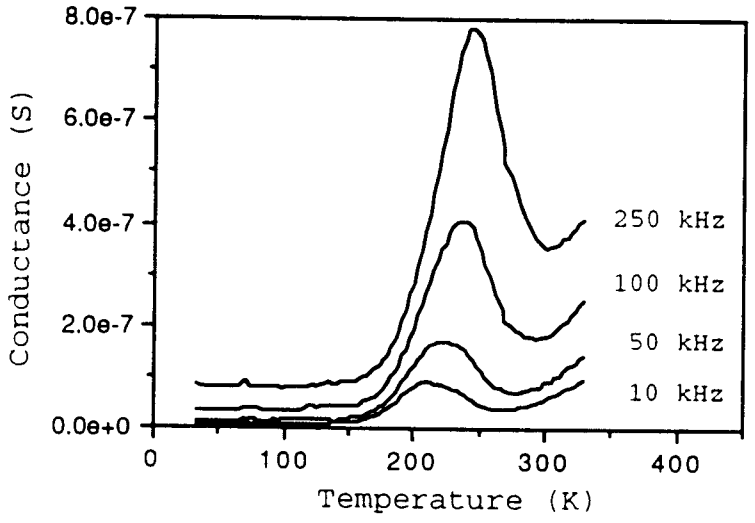

Figure 3.5. Conductance versus temperature plot at various frequencies from DLAS measurements.

In the G versus T plot, the conductance peak's position and peak height is frequency dependent. The conductance peak appears at a temperature corresponding to the activation

energy (E_a) of a particular trap. Thus, from eqns. (3.7), (3.8), and (3.9), the activation energy (E_a, eV) and the capture cross section (σ, cm^2) can be obtained from a $\ln(\frac{\omega}{T^2})$ versus $\frac{1}{T}$ plot.

$$e = \sigma V_{th} N_c \exp\left(\frac{-E_a}{KT}\right) \tag{3.7}$$

where, e = thermal emission rate (sec^{-1}), σ = capture cross section (cm^2), V_{th} = thermal velocity (cm/sec), N_c= effective density of states on the conduction band, E_a = activation energy (eV), K = Boltzmann's constant. Since

$$e = \omega = 2\pi f \ , \ V_{th} = A\ T^{1/2} \ , \ N_c = B\ T^{3/2}$$

where, ω is the angular frequency, f is frequency, $A = (\frac{3K}{m^*})^{1/2}$, and $B = (\frac{2\pi m^*}{h^2})^{3/2}$,

$$e = \omega = \sigma A\ B\ (\ T^2)\ \exp\left(\frac{-E_a}{KT}\right) \ . \tag{3.8}$$

Taking the logarithm of eqn. (3.8) gives

$$\ln \frac{\omega}{T^2} = \left(\frac{-E_a}{K}\right)\left(\frac{1}{T}\right) + \ln\ (\ \sigma\ A\ B\ ) \ . \tag{3.9}$$

Thus, the conductance versus temperature plot results in peaks corresponding to deep levels. The corresponding effect

observed in the capacitance versus temperature characteristic is the appearance of step-like variations in the capacitance; these steps appear near the temperature of the conductance peaks. Identifying capacitance changes as due to the excitation of the traps, the corresponding trap concentration (N_t) is calculated as follows:

$$\frac{N_t}{N_d} = \frac{(C_0^2 - C^2(T))}{C_0^2} \cong \frac{2\Delta C}{C_0} \qquad (3.10)$$

where, N_t = the concentration of a particular trap level, N_d = donor concentration (for a p^+n junction), C_0 = the capacitance under zero bias at room temperature, C(T) = the capacitance at the top of a step for a particular trap at temperature T, and $\Delta C = C_0 - C(T)$.

The DLAS measurement system, as shown in Fig. 3.6, consists of: (1) variable temperature cryostat (35 °K ~ 370 °K), (2) vacuum pump (TRIVAC model D2A), (3) compressor module (model HC-4), (4) programmable temperature controller (R. G. Hansen & Associates Series 8000), (5) HP 9000 series 236 and HP 9133 computers, and (6) HP 4192A LF impedance analyzer (5 Hz ~ 13 MHz).

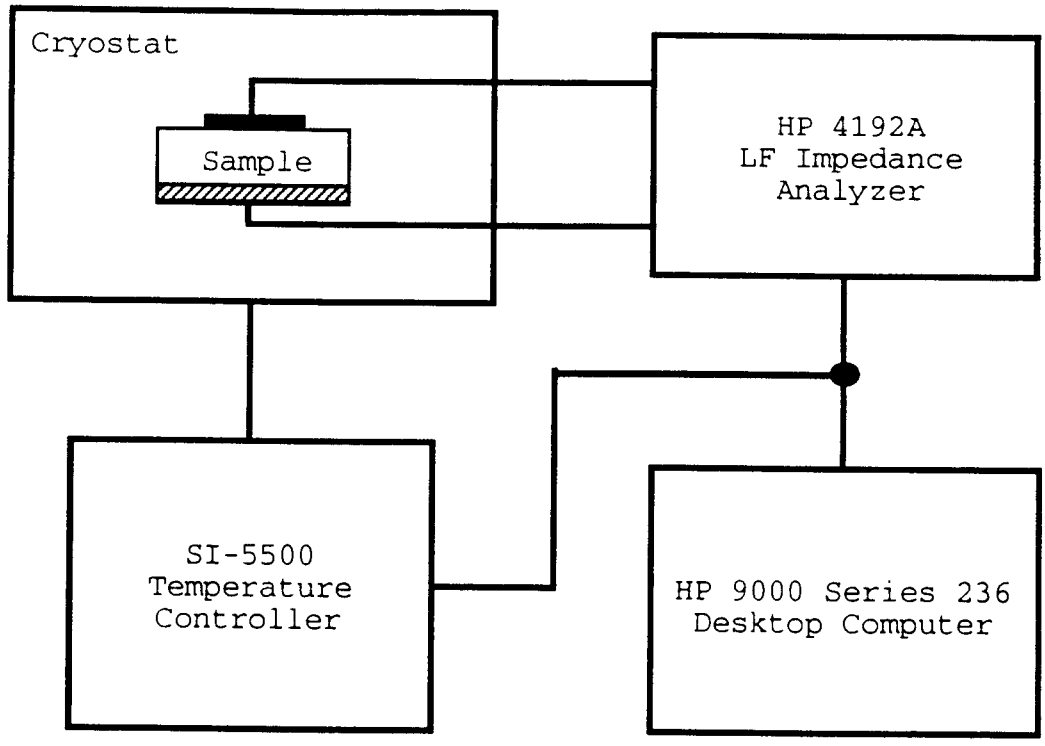

Figure 3.6. Schematic setup for DLAS measurements.

3.3. Thermally Stimulated Capacitance

Thermally stimulated capacitance (TSCAP) originated with Carballes and Lebailly [64]. This technique was originally used for insulators and later adapted to lower resistivity semiconductors when it was recognized that the reversed-bias space-charge region (scr) is a region of high resistance [65]. During the measurement the device is cooled and traps are filled with majority carriers at zero bias. Alternatively, traps can be filled with minority carriers by optical injection or by forward biasing a pn junction. Then the device is reverse biased, heated at a constant rate, and

the steady-state capacitance is measured as a function of temperature.

In most cases the trap (or, deep level) concentration, N_t, is a large fraction of the net donor concentration, Nd, and is proportional to N_d even at rather high doping levels. Thus, the relative capacitance change $\Delta C/C$ due to carrier trapping at (or, emission from) deep levels in the depletion region of a pn junction or Schottky barrier is of the order of unity. In this large-signal limit the usual simple analysis methods used to obtain the defect concentration from DLTS spectra are inadequate. TSCAP is a somewhat better diagnostic tool to study concentrations and slow metastable effects in such a system.

The procedures used in establishing the initial conditions for the three C(T) curves in Fig. 3.7 are as follows:

(1) Curve 1 is the steady-state zero-bias capacitance recorded as a function of temperature and it is reversible for increasing or decreasing temperature scans. Curves 2 and 3, on the other hand, are irreversible thermal scans corresponding to initial conditions at the lowest temperature of completely filled or completely empty deep levels, respectively.

(2) Initial condition 2 is obtained by cooling the sample from 300 °K to about 77 °K with +1 V bias. This bias corresponds to a narrowing of the junction space-charge region (scr) so that nearly all deep levels are below the

Fermi level and hence filled with electrons (neutral charge state). At the lowest temperature the bias is returned to 0 V where the filled deep levels in the scr constitute a nonequilibrium state which is metastable because the electron thermal emission rate is vanishingly small at 77 'K. Thus, as shown in Fig. 3.8(a), the scr of width W_2 is made up only of ionized "normal" (shallow) donors of net concentration Nd since deep levels are frozen out at 77 'K. When the

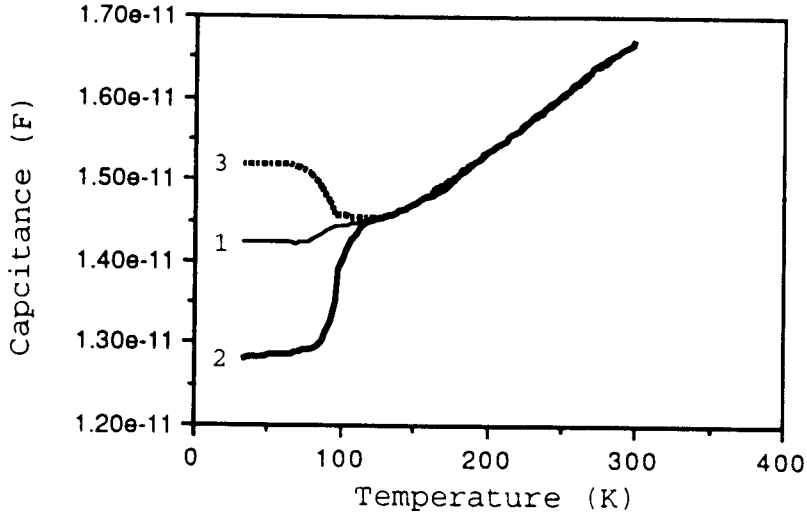

Figure 3.7. TSCAP scans showing three C(T) curves for three difference initial conditions.

temperature is increased to the vicinity of 100 'K, the deep levels begin to thermally emit their trapped electrons and hence become positively charged. Since $N_t >> N_d$ in most cases, this corresponds to a drastic rearrangement of the space charge at constant bias which finally results in the equilibrium width W_1, shown in Fig. 3.8(a) as the step-wise

charge distribution with shaded boundaries (in the abrupt-depletion approximation). The step at $(W_1 - \lambda)$ corresponds to the point where the deep level passes through the Fermi level within the scr. Thus, between 0 and $(W_1 - \lambda)$, the deep levels are above the Fermi level and are empty in equilibrium so that the positive space charge is $q(N_T + N_d)$. In the region $(W_1 - \lambda)$ to W_1, the energy level of the deep levels is below the Fermi level so that the equilibrium space charge is only qN_d. The steady-state capacitance change of curve 1 as a function of temperature corresponds primarily to the temperature dependence of the Fermi level, and consequently of λ. As λ changes with temperature at constant-bias voltage, the space-charge distribution, and hence W_1 in Fig. 3.8(a), must change accordingly.

(3) Initial condition 3 in Fig. 3.7 corresponds to all deep levels empty. This is illustrated in Fig. 3.8(a) with the space-charge distribution $q(N_T + N_d)$ from 0 to W_3. Condition 3 is obtained at low temperature from steady-state condition 1 by emptying the deep levels either optically, by exciting the electrons to the conduction band, or electrically, by recombination of the electrons with injected holes under forward bias. The optical emptying path is illustrated in Fig. 3.7 and is utilized in the photocapacitance method to measure the electron photoionization cross section $\sigma_n^*(h\nu)$ [2], as shown in Fig. 3.8(b).

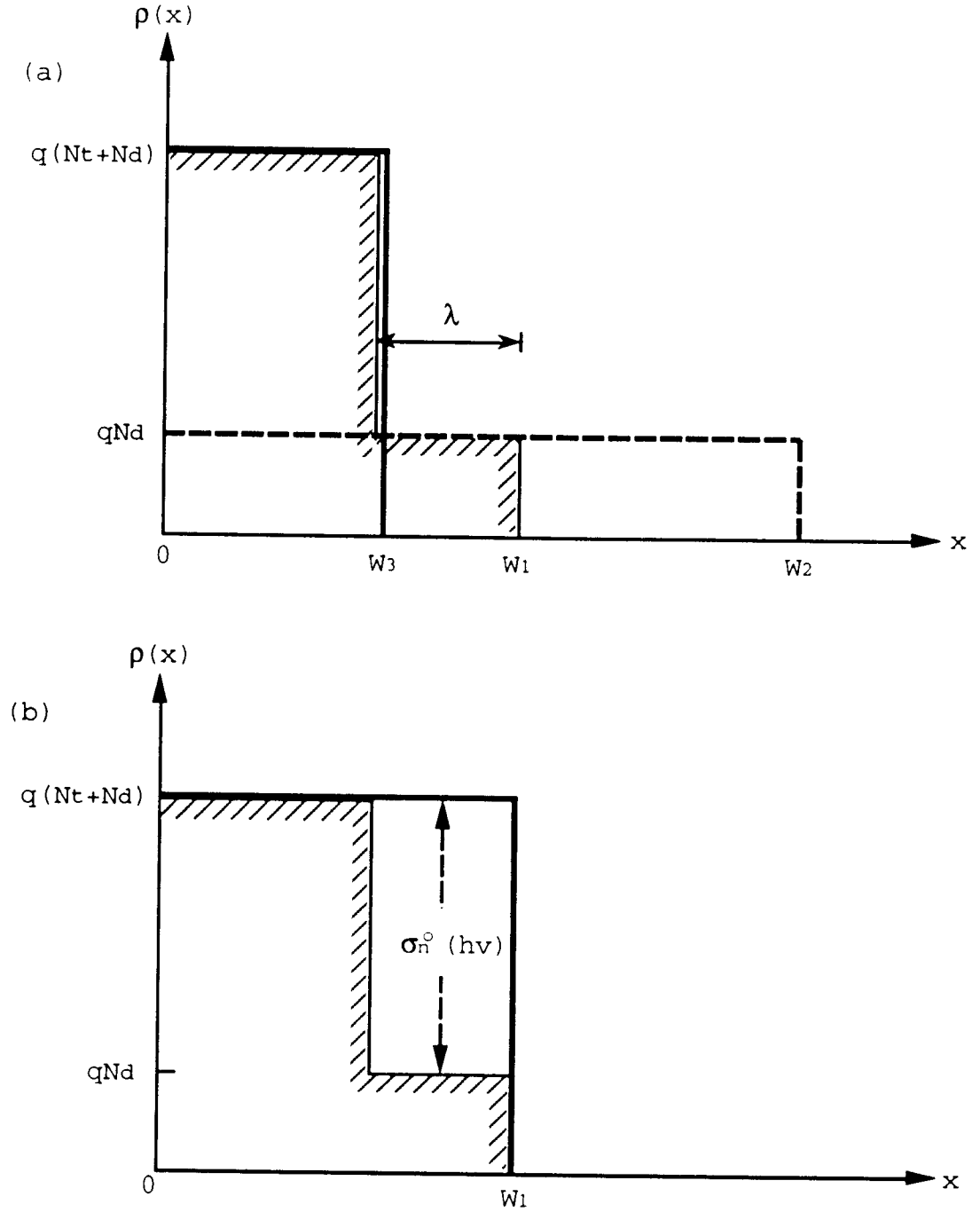

Figure 3.8. Illustration of the charge density variation (a) for three initial conditions as described in Fig. 3.7 and (b) for the constant-capacitance condition of photoionization measurements [20].

The positive-going TSCAP step, corresponding to initial condition 2 is the same physical phenomenon (thermal electron emission) as gives rise to the negative DLTS peak. From the magnitude of the TSCAP step, one can calculate the concentration of the deep levels which are emitting electrons with rates of the order of seconds in the temperature range of the step. Similarly, the negative-going TSCAP step, corresponding to initial condition 3, arises from the same effect as the positive DLTS peak, electron capture.

Usually, a positive DLTS peak or a negative-going TSCAP step is due to minority-carrier emission (holes in this case). However, the fact that initial condition 3 can be established in an n-type Schottky barrier by illumination with photons of energy as low as, say, 0.6 eV for DX centers in Te-doped AlGaAs totally rules out the possibility of hole emission in this temperature range, since a photon energy greater than 1.5 eV would be needed to empty hole traps close enough to the valence band to emit holes at the same temperature as the positive DLTS peak.

The capacitance values corresponding to conditions 1, 2, and 3 in Fig. 3.7 can be used to determine the trap (or, deep level) and the net shallow donor concentrations. The concentration of the traps is assessed by [2]

$$\frac{N_t}{Nd} = \left(\frac{C_3}{C_2}\right)^2 - 1 \qquad (3.11)$$

where C_2 and C_3 indicate the capacitance values at 77 °K of curve 2 and 3, respectively.

The TSCAP setup is identical to the DLAS setup shown in Fig. 3.6.

3.4. Capacitance-Voltage Measurement

The capacitance-voltage (C-V) technique relies on the fact that the width of a reversed-biased space-charge region (scr) of a semiconductor junction device depends on the applied voltage. The C-V profiling method has been used with Schottky barrier diodes, p-n junctions, MOS capacitors, and MOSFETs.

Consider the Schottky barrier diode of Fig. 3.9. The semiconductor is p-type with a doping concentration N_A. A d.c. bias, V, is applied to the metal contact. The reverse bias produces a space-charge region of width W. The capacitance is defined as

$$C = - \frac{dQ_S}{dV} \tag{3.12}$$

where Q_S is the semiconductor charge. The negative sign accounts for more negative charge in the semiconductor scr (that is, negatively charged ionized acceptors) for an increased positive voltage on the metal.

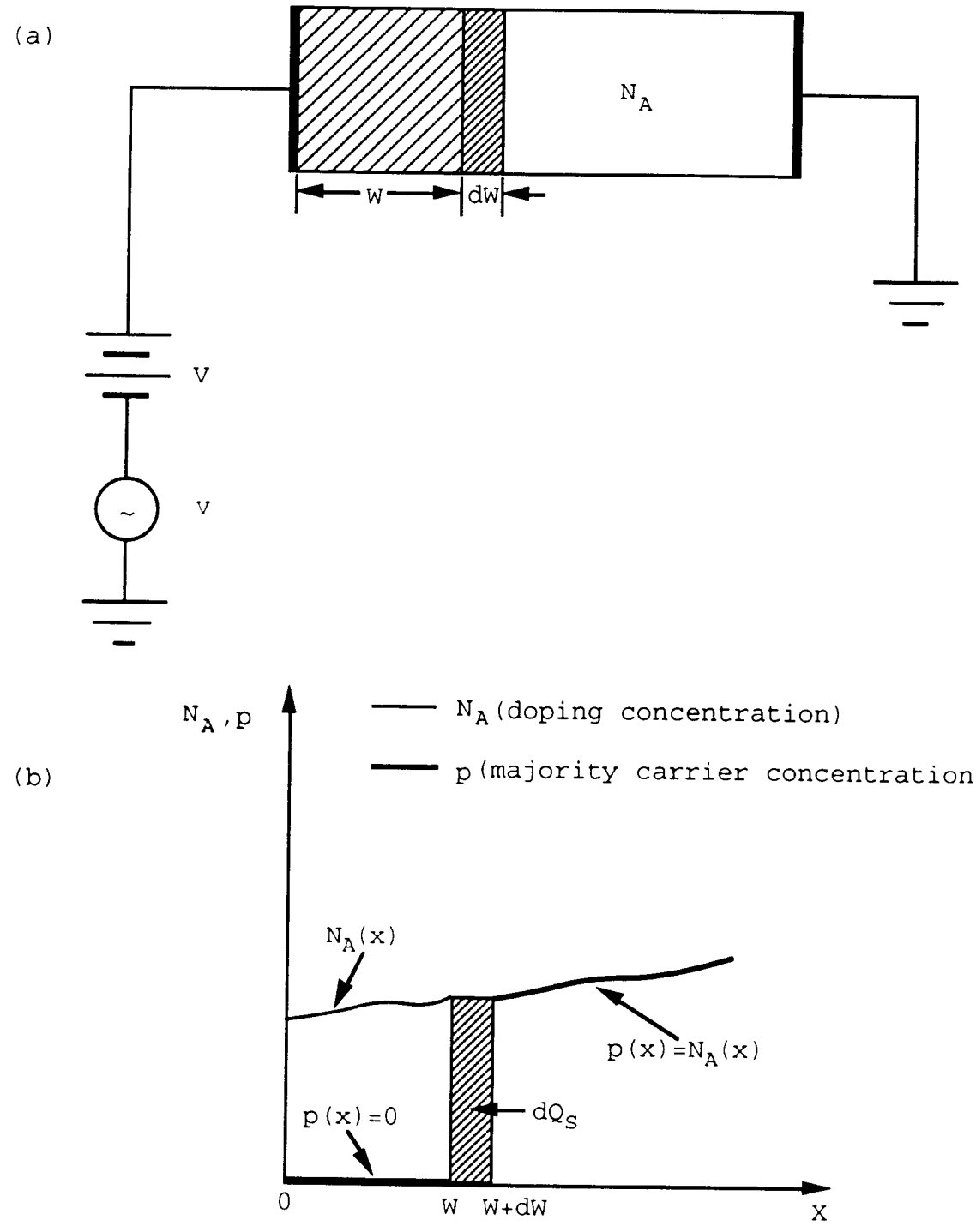

Figure 3.9. (a) A reversed-biased Schottky diode and (b) the doping concentration (NA) and majority carrier (p) profiles in the depletion approximation [1].

The capacitance is determined by superimposing a small-amplitude ac voltage, v, on the d.c. voltage V. Typically, the ac voltage varies at a frequency of 1MHz with an amplitude of 10 to 20 mV, but other frequencies and voltages can be used. Consider the diode to be biased to a d.c. voltage V plus a sinusoidal ac voltage. Imagine that the ac voltage increases from zero bias to a small positive voltage, thus adding a charge increment, dQ_m, to the metal contact. The charge increment dQ_m must be balanced by an equal semiconductor charge increment, dQ_S, for overall charge neutrality, where dQ_S is given by

$$dQ_S = -qAN_A(W)dW \tag{3.13}$$

where W is the space-charge region width and dW is the scr width increment. Thus, from eqns. (3.12) and (3.13),

$$C = -\frac{dQ_S}{dV} = qAN_A(W)\frac{dW}{dV} . \tag{3.14}$$

Also, the capacitance of a reverse-biased junction, when considered as a parallel plate capacitor, is expressed as

$$C = \frac{K_S\varepsilon_0 A}{W} . \tag{3.15}$$

Taking the reciprocal of eqn. (3.15) and arranging it gives

$$W = \frac{K_S \varepsilon_0 A}{C} \quad . \tag{3.16}$$

Differentiating eqn. (3.16) with respect to voltage and substituting dW/dV into eqn. (3.14) gives

$$N_A(W) = - \frac{C^3}{qK_S \varepsilon_0 A^2 (dC/dV)} \quad , \tag{3.17}$$

which can also be written as

$$N_A(W) = \frac{2}{qK_S \varepsilon_0 A^2 [d(1/C^2)/dV]} \tag{3.18}$$

by using the identity $\frac{d(1/C^2)}{dV} = -(2/C^3)\frac{dC}{dV}$.

From eqn. (3.15), we find the scr width dependence on capacitance is given by

$$W = \frac{K_S \varepsilon_0 A}{C} \quad . \tag{3.19}$$

Equations (3.18) and (3.19) are the key equations for obtaining doping profiling from the C-V technique.

The doping concentration is obtained from a C-V curve by taking the slope dC/dV from eqn. (3.17) or by plotting $1/C^2$ versus V and taking the slope $d(1/C^2)/dV$ from eqn. (3.8).The depth at which the doping concentration is evaluated may be

obtained from eqn. (3.19). For a Schottky barrier diode there is no ambiguity in the scr width since it can only spread into the substrate; space-charge region spreading into the metal is totally negligible.

The doping profile theory is equally applicable for asymmetrical pn junctions with one side of the junction more heavily doped than the other. Such junctions are generally referred to as p^+n or n^+p junctions. If the doping concentration of the heavily doped side is 100 or more times higher than that of the lowly doped side, then scr spreading into the heavily doped region can be neglected, and eqns. (3.18) and (3.19) hold. If that condition is not met, the equations must be modified or both doping concentration and depth will be in error [66]. The correction, however, is difficult and it has been proposed that no unique doping profile can be derived from C-V measurements under these conditions [67]. If the doping profile of one side of the the junction is known, then the profile on the other side can be derived from C-V measurements [68]. Fortunately, most pn junctions utilized for doping concentration profiling are of the p^+n or n^+p type and, hence, corrections due to doping asymmetries are not required.

The depletion approximation is used for the derivation of eqn. (3.18), which completely neglects minority carriers and assumes a total absence of majority carriers in the space-charge region with a depth W and perfect charge neutrality beyond W. Generally, this is a reasonably good

approximation when the scr is reverse biased and when the substrate is uniformly doped. Furthermore the acceptor concentration at the edge of the space-charge region is used as the incremental charge variation. The a.c. voltage exposes more or less ionized acceptors at the scr edge as shown in Fig. 3.9. The charges that actually move in response to the ac voltage are the mobile holes rather than acceptor ions. From this point of view, the differential C-V profiling technique determines the majority carrier concentration (p) not the doping concentration (N_a) and the relevant equations become [1]

$$p(W) = \frac{2}{qK_S\varepsilon_0 A^2[d(1/C^2)/dV]} \qquad (3.20)$$

$$W = \frac{K_S\varepsilon_0 A}{C} \ . \qquad (3.21)$$

3.5. Current versus Voltage Measurements

I-V measurements at room and low (77 °K) temperatures were performed to characterize samples using an HP 4145B semiconductor parameter analyzer and a probe station.

Chapter 4. DX Centers in AlGaAs Heterojunction Bipolar Transistors

4.1. Introduction

In this chapter, characterization of the DX center in the AlGaAs emitter region of an HBT by DLTS, DLAS, TSCAP, and C-V profiling measurements is presented. In these measurements, the base and the collector are connected together and grounded while the emitter is biased; thus the HBT acts as a diode. Also, a discussion of the effect of the DX center on HBT performance is provided.

4.2. Experimental Results

The n-AlGaAs layers studied were the emitter junctions of HBTs and were grown by MBE at Tektronix at a substrate temperature of 630 °C. The base and collector of the HBT were connected together and grounded. The MBE grown epitaxial layer structure is given in Table 4.1 [72]. Among the layers, the cap layer was grown to aid the formation of ohmic contacts [73]. Compositional grading layer of the emitter to base region was employed to smooth out the conduction band discontinuity (spike) and so reduce the emitter-base junction turn-on voltage [74] and, therefore, alleviate the need for a double heterojunction structure. The spacer layer was used to reduce the emitter-base space-charge recombination [75] and

Layer	Aluminum Composition	Dopant	Doping (cm^{-3})	Thickness (Å)
Cap	0	Si	$5x10^{18}$	1000
Graded	0~0.25	Si	$5x10^{17}$	300
Emitter	0.25	Si	$5x10^{17}$	1000
Graded	0.25~0	Si	$5x10^{17}$	300
Spacer	0	-	-	100
Base	0	Be	$2x10^{19}$	1000
n^-Collector	0	Si	$3x10^{16}$	5000
n^+Collector	0	Si	$5x10^{18}$	5000
Substrate	0	-	S.I.	508 (μm)

Table 4.1. MBE grown epitaxial HBT structure [72].

to act as a buffer against surface diffusion of Be [76].

4.2.1. Capacitance versus Voltage

C-V measurements are performed by increasing the applied voltage from -5 V to 0 V using a step of 0.1 V and monitoring the corresponding capacitance. Using eqns. (3.20) and (3.21), the doping profile is obtained as shown in Fig. 4.1. It is seen that the donor concentration near the p-n junction remains constant and then increases at a distance of 0.15 μm from the junction. This change in the doping concentration is associated with the transition from the emitter to the graded layer ($5x10^{17}$ cm^{-3}) to the cap layer ($5x10^{18}$ cm^{-3}), as indicated in Table 4.1.

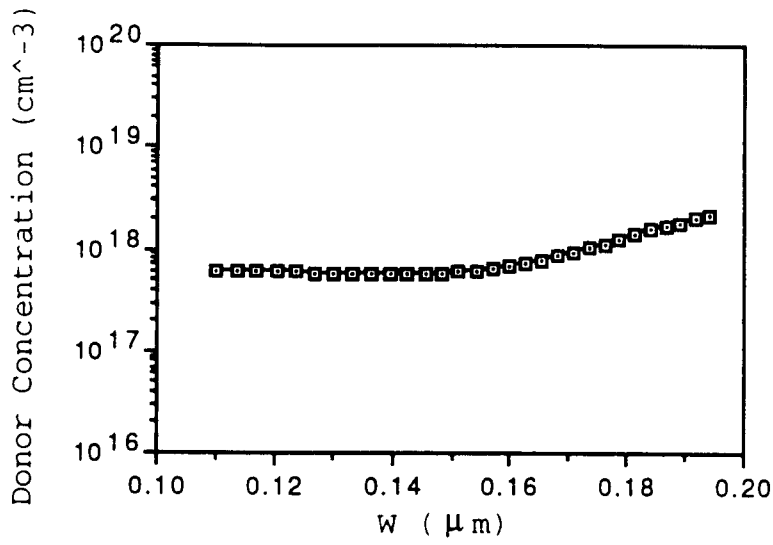

Figure 4.1. The doping profile from C-V measurement.

4.2.2. Thermal Stimulated Capacitance

As shown in Fig. 4.2, TSCAP curve 1 was initialized by cooling the sample from 300 °K to 40 °K under zero bias; the sample was then heated at a constant rate to 300 °K to obtain the steady-state zero bias capacitance, i.e. curve 1. Curve 2 was obtained by cooling the sample from 300 °K to 40 °K while applying a +1.2 V bias to fill deep donor levels; when the temperature reached 40 °K, the bias was changed to 0 V and then the sample was heated at a constant rate to 300 °K. Curve 3 was initialized as curve 1; however, at 40 °K, a forward bias of +1.4 V was applied and the sample was then heated to 300 °K under this forward bias. The purpose of the forward bias was to empty deep levels since deep levels are emptied by the recombination of electrons with injected holes (minority

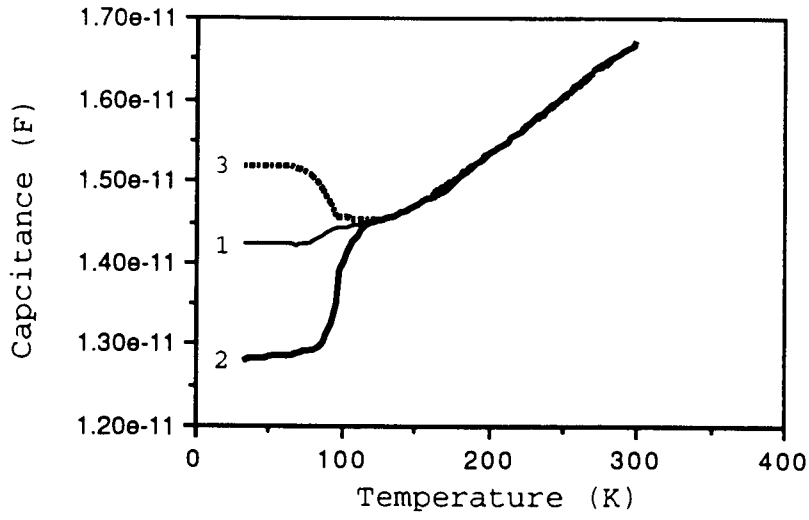

Figure 4.2. Capacitance versus temperature plot from TSCAP measurements.

carrier emission) [1,20]. From the capacitance values of curve 3 and curve 2 at 77 °K, the trap concentration, N_t, was estimated to be 2.03×10^{17} cm^{-3}, using eqn. (3.11).

4.2.3. Deep Level Admittance Spectroscopy

DLAS measurements are performed by measuring the conductance (G) as a function of temperature (T) at frequencies of 250, 100, 50, and 10 kHz, as shown in Fig. 4.3. The Arrhenius plot shown in Fig. 4.4 was then obtained using eqn. (3.9), yielding an activation energy 0.386 eV and a capture cross section of 5.58×10^{-13} cm^2.

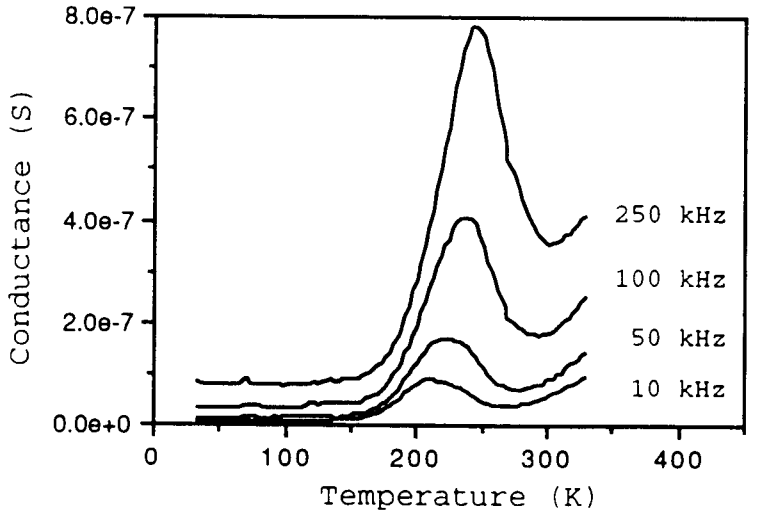

Figure 4.3. DLAS measurements at frequencies 250, 100, 50, and 10 kHz.

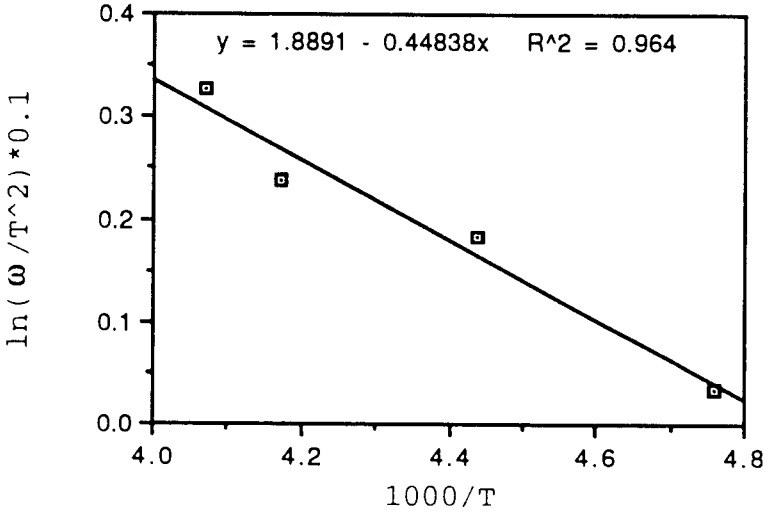

Figure 4.4. DLAS Arrhenius plot corresponding to Fig. 4.3.

4.2.4. Deep Level Transient Spectroscopy

Figures 4.5 and 4.7 illustrate DLTS spectra observed under a rate window width of 0.1 msec using a filling pulse width of 50 msec and a rate window width of 10 msec using a filling pulse width of 30 msec, respectively. Arrhenius plots corresponding to different DX levels are shown in Figs. 4.6, 4.8, and 4.9.

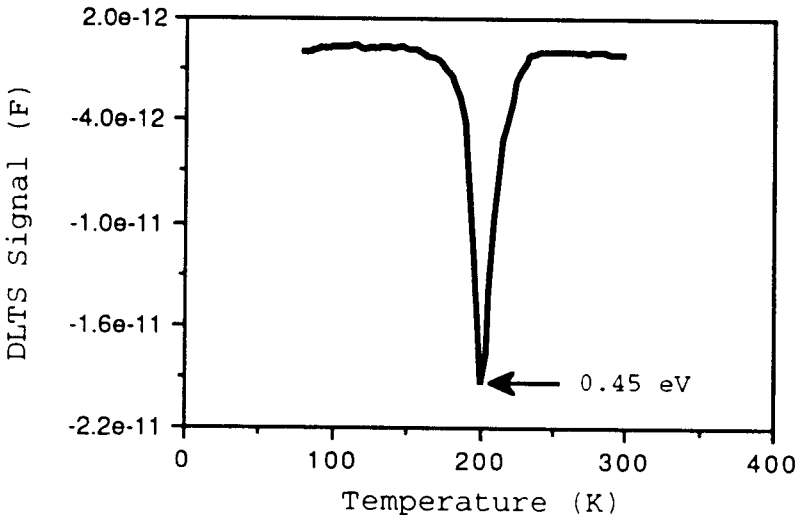

Figure 4.5. DLTS spectra using a rate window width of 0.1 msec and a filling pulse width of 50 msec.

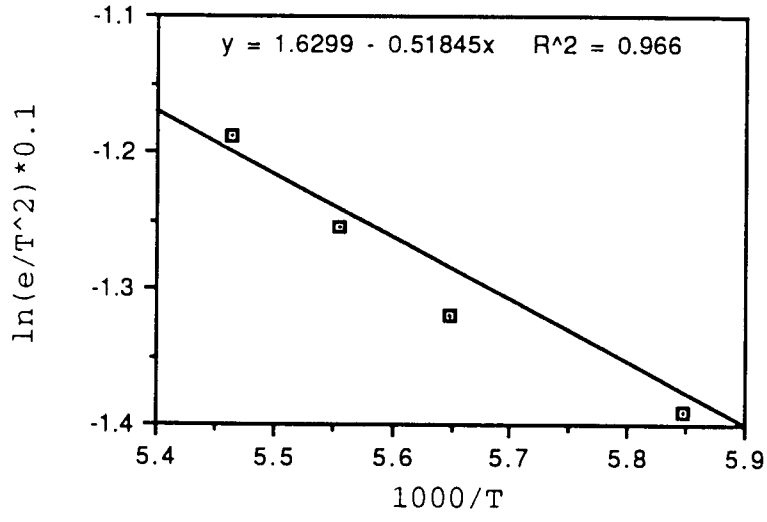

Figure 4.6. DLTS Arrhenius plot corresponding to Fig. 4.5.

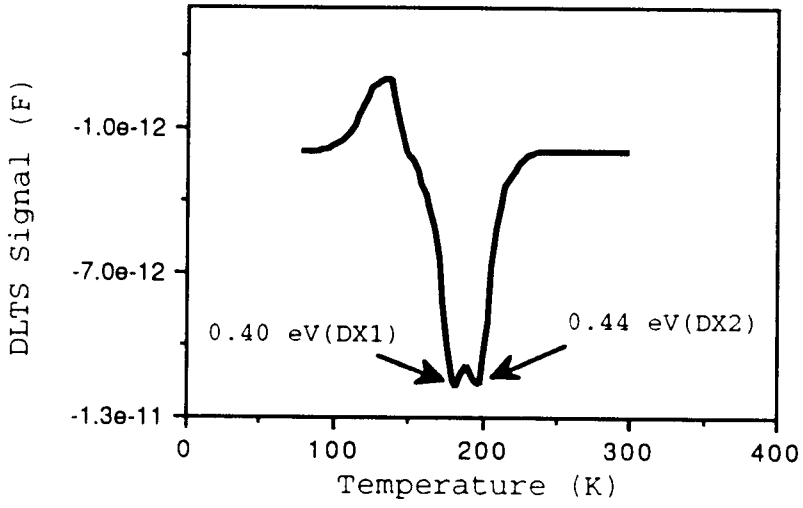

Figure 4.7. DLTS spectra using a rate window width of 10 msec and a filling pulse width of 30 msec. Two deep levels, denoted DX1 and DX2, are observed.

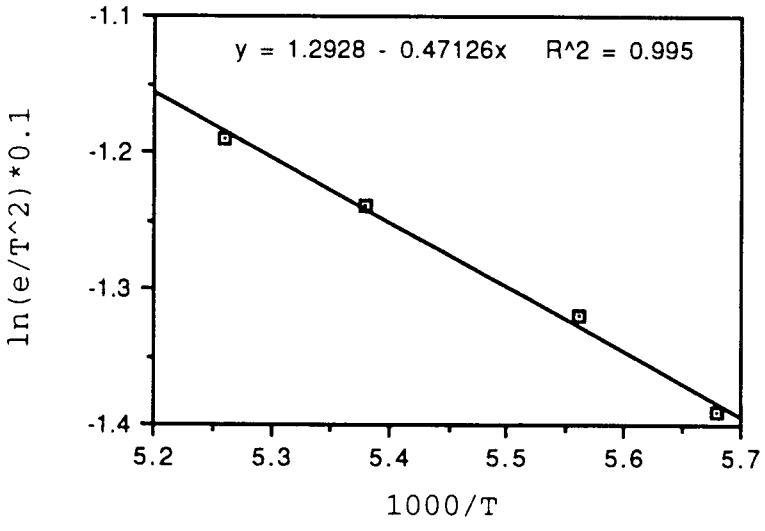

Figure 4.8. Arrhenius plot for DX1 of Fig. 4.7.

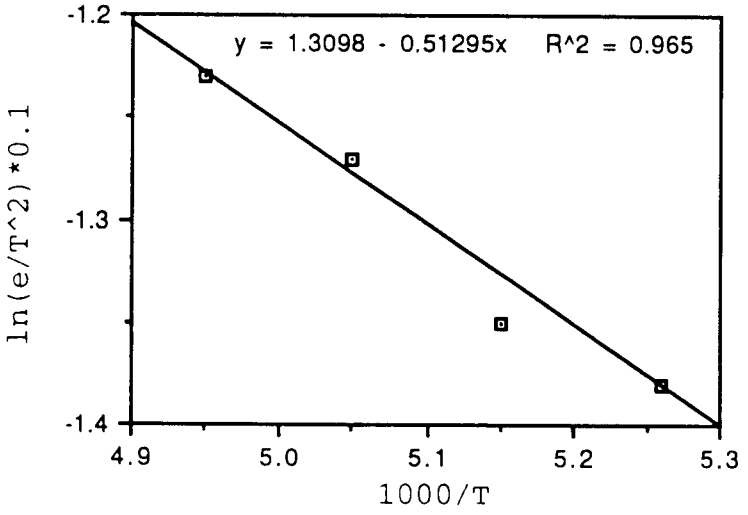

Figure 4.9. Arrhenius plot for DX2 of Fig. 4.7.

4.2.5. A Comparison of Results from Various Characterization Methods

A comparison of results from different characterization methods is given in Table 4.2. The activation energies measured by DLTS are close to previously reported DX values, as listed in Table 2.1 [21]. However, the value of E_a obtained from DLAS measurements was substantially smaller than previously reported DX activation energies. This may be due to the frequencies employed (i.e., 250, 100, 50, and 10 kHz) which are much larger than the capture rate of the DX center, precluding the attainment of steady state in the DLAS measurement. The variance in the measured capture cross sections is consistent with the results of Calleja *et al.* showing that different DX's have different capture cross sections but the same activation energy [91].

The DX concentration deduced by DLTS is about one half

Methods	Ea (eV)	σ (cm^2)	Nt (cm^{-3})
DLTS (DX)	0.447	4.18×10^{-14}	2.31×10^{17}
DLTS (DX_1)	0.404	1.43×10^{-15}	–
DLTS (DX_2)	0.439	1.80×10^{-15}	–
DLAS	0.386	5.58×10^{-13}	–
TSCAP	–	–	2.03×10^{17}

Table 4.2. A comparison of results obtained from various characterization methods.

of the measured doping concentration. This result is consistent with Chadi and Chang's negative U model for DX. The TSCAP-deduced concentration is slightly smaller than that measured by DLTS. This may be due to an incomplete emptying of the deep levels during the initialization of curve 3, Fig. 4.2.

4.3. Discussion

4.3.1. DLTS Analysis

4.3.1.1. The Positive Peak in DLTS Spectra

Figure 4.7 shows that there is a positive peak at about 120 °K in the DLTS signal corresponding to minority carrier emission from a deep trap; however, this minority trap is not detected by DLAS. Using eqns. (4.1) and (4.2), as follows, to evaluate the time for electron capture, τ_c:

$$\tau_c = \frac{1}{c} = \frac{1}{\sigma V_{th} n} \qquad (4.1)$$

$$\sigma = \sigma_\infty \exp\left(\frac{-E_{cap}}{KT}\right) \qquad (4.2)$$

where, c = capture rate (sec), V_{th} = thermal velocity, σ = capture cross section at temperature T, σ_∞ = high temperature capture cross section, and E_{cap} = capture energy. For E_{cap} = 0.21 eV in Si-doped AlGaAs [21] and $\sigma_\infty = 10^{-14}$ cm^2

[20], at 120 °K, σ is calculated to be 1.51×10^{-23} cm^2. Substituting this value of σ value into eqn. (4.1), using V_{th} = 10^7 cm/sec and n = 5×10^{-17} cm^{-3}, τ_c is equal to 1.32×10^{-2} sec. Thus, τ_c is in the same range as the rate windows employed in the DLTS measurement. Hence, it is concluded that the positive peak observed in Fig. 4.10 is an experimental artifact, not minority carrier deep level emission, which arises from this sluggish rate of electron capture characteristic of the DX center. This positive peak experimental artifact is due to the peculiar nature of the DX center, i.e., its electron capture cross section is very small and thermally activated at low temperature (120 °K). Note that this conclusion is consistent with the observation that when a rate window larger than the low-temperature capture rate is used, this positive DLTS peak disappears.

4.3.1.2. The Deep Level with an Activation Energy of 0.75 eV

Two dominant deep electron traps, E_a = 0.45 eV and E_a = 0.75 eV, are typically observed in Si-doped AlGaAs grown by MBE. The first deep level with E_a = 0.45 eV is identified as DX, as shown in Fig. 4.10. The E_a = 0.75 eV deep level is found [82] to be present at a concentration independent of the doping concentration (in contrast to DX). It is likely that this E_a = 0.75 eV trap is EL2, another peculiar deep level with metastable properties. EL2 is believed [55,56] to be an arsenic antisite which undergoes a LLR, similar to the DX center, when exhibiting metastable characteristics.

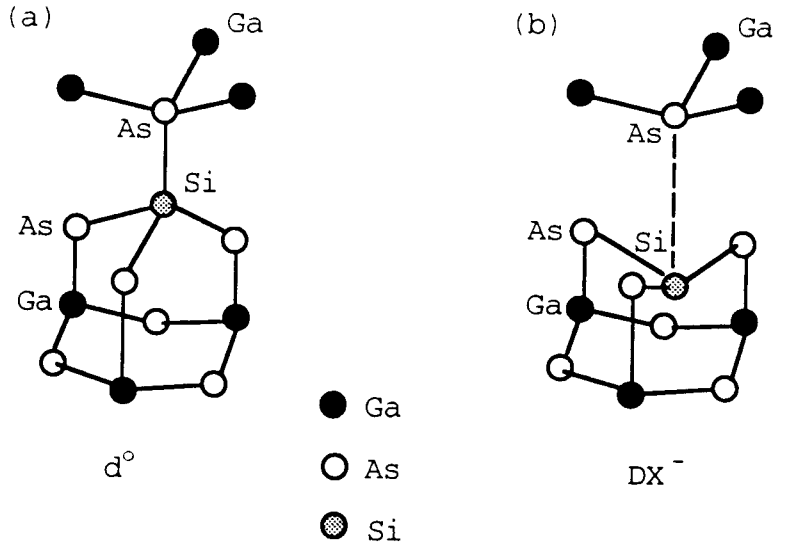

Figure 4.10. Negative U model for the DX center in Si-doped AlGaAs in (a) the normal substitutional site and (b) the broken bond configuration.

However, in the DLTS measurements performed herein, only one deep level is observed with E_a = 0.45 eV (actually, two closely spaced deep levels with E_a = 0.40 and 0.44 eV, are observed and are believed to comprise part of a DX family).

The absence of the E_a = 0.75 eV deep level is consistent with observations [81] indicating that the concentration of this deep level decreases rapidly with increasing substrate growth temperature and is negligible when the $Al_{0.25}Ga_{0.75}As$ growth temperature is above 630 °C. At an AlGaAs growth temperature of 630 °C, the concentration of E_a = 0.75 eV is estimated to be about one hundredth of the concentration of DX [81].

4.3.1.3. Inter-dependence of DX_1 and DX_2

Figures 4.5 and 4.7 show that the deep trap E_a = 0.45 eV is actually comprised of two close deep traps, DX_1 and DX_2. The existence of multiple DX peaks is attributed to the fact that Si moves to an interstitial, antibonding site upon electron capture into the metastable DX state [55,56]. In this configuration, Fig. 4.10, the neighboring cation could be either Ga or Al, and the DLTS peaks would correspond to local environments having 0, 1, 2, or 3 Al atoms; this provides an explanation for the fact that several (two or three) close peaks are observed [92]. Also, the presence of these two peaks is consistent with the observation of only two peaks for $0.14 < x < 0.27$ since, at low Al composition, the local environment of DX is likely to contain 0 or 1 Al atom [92]. These two deep levels DX_1 and DX_2 are estimated to have activation energies of 0.40 and 0.44 eV, respectively, in the work described herein and also by other investigators [22,79].

In Fig. 4.11, it is shown that the relative magnitude of the peak heights DX_1 and DX_2 is a function of the DLTS rate window width. While the magnitude of peak DX_1 is approximately unchanged, peak DX_2 decreases with increasing rate window width as these peaks shift to lower temperatures.

The dependence of the DLTS peak heights of DX_1 and DX_1 on the filling pulse width is shown in Fig. 4.12. This figure indicates that as the filling pulse width increases the

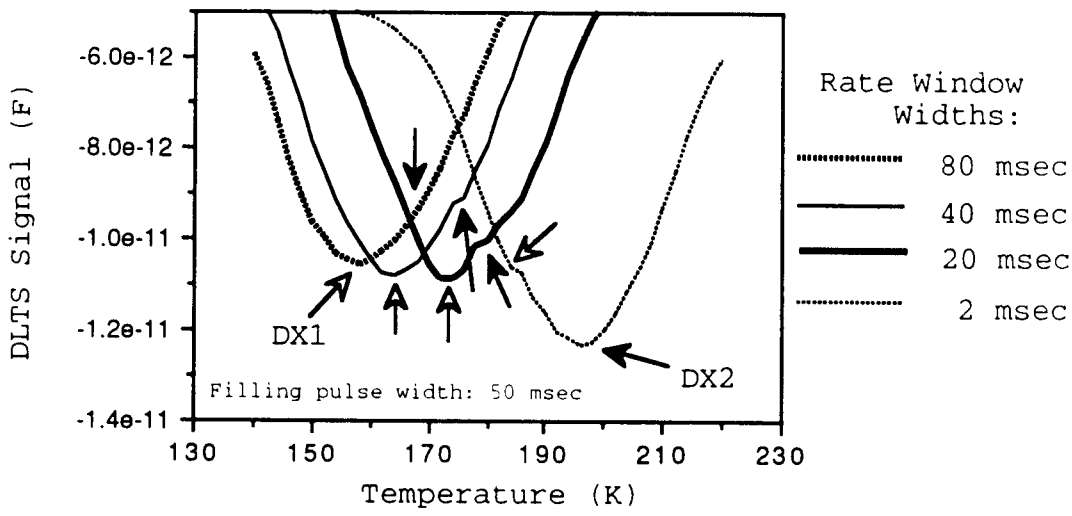

Figure 4.11. Deep levels DX1 and DX2 for various rate window widths.

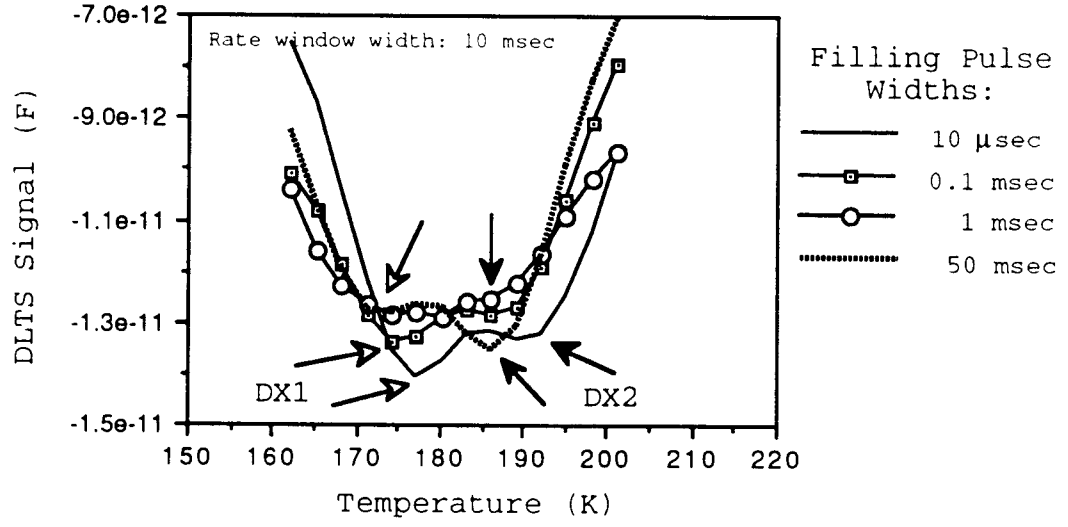

Figure 4.12. Deep levels DX1 and DX2 for different filling pulse widths.

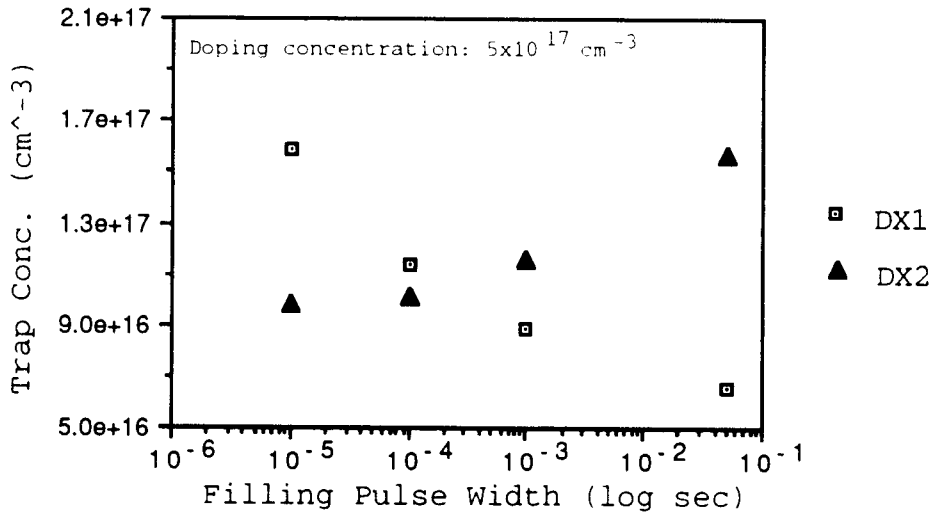

Figure 4.13. Concentrations of deep levels DX1 and DX2 as a function of filling pulse width.

magnitude of peak DX_2 increases whereas the magnitude of peak DX_1 correspondingly decreases. The concentrations of DX_1 and DX_2 as a function of filling pulse width are shown in Fig. 4.13.

Although these two DX centers are estimated to have different activation energies in the work described herein and in work reported by other researchers [22,79], recent DLTS data analysis [91] by Calleja *et al.* indicates DX_1 and DX_2 to have identical activation energies but different capture cross sections. This conclusion is obtained by curve fitting DLTS capacitance transient curves using multiple exponentials and performing an Arrhenius analysis on each current curve-fit exponential individually. The work of Calleja *et al.* emphasizes that data analysis of non-exponential DLTS transient curves must be undertaken with

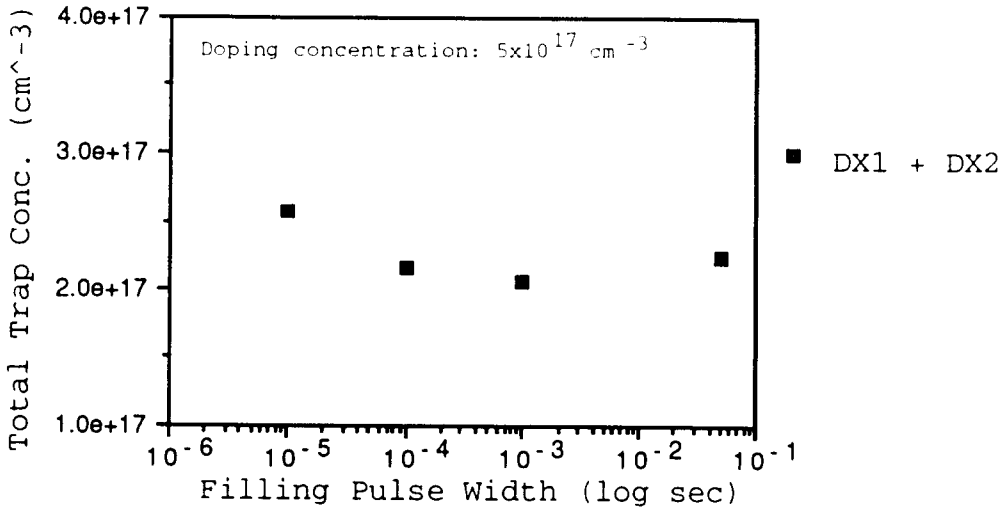

Figure 4.14. Total trap concentrations of DX_1 and DX_2 versus filling pulse widths.

extreme care if unequivocal quantitative conclusions are to be reached.

The total trap concentration versus filling pulse width is shown in Fig. 4.14. This figure indicates that the DX concentration is almost constant as a function of filling pulse width and is about 50% ~ 60% of the doping concentration; this is consistent with the negative-U model of the DX center [55,56].

4.3.2. The Effect of the DX Centers on the Performance of HBTs

4.3.2.1. Current Gain (β) at Low Collector Current

A plot of the current gain, β, of an HBT as a function of the collector current, I_c, is given in Fig. 4.15. Note

that β is only about 40 at low collector current (I_c = 0.2 mA). The recombination current (I_r) caused by DX centers is given by [89,90]

$$I_r = \frac{AqN_tW_{scr}}{\tau_c} \qquad (4\text{-}8)$$

where, A is the area of the junction, N_t is the density of traps, W_{scr} is the depletion region width, and τ_c is the time for the DX center to capture an electron. At 300 °K, for A = $1x10^{-4}$ cm^2, N_t = $2.5x10^{17}$ cm^{-3}, W_{scr} = 450 Å at +1 V, and τ_c = $1.35x10^{-7}$ sec, the recombination current is estimated to be approximately 0.13 mA which is not negligible compared to I_c = 0.2 mA. Thus, the observed reduction in β at small I_c's is attributed to DX recombination in the emitter/base scr.

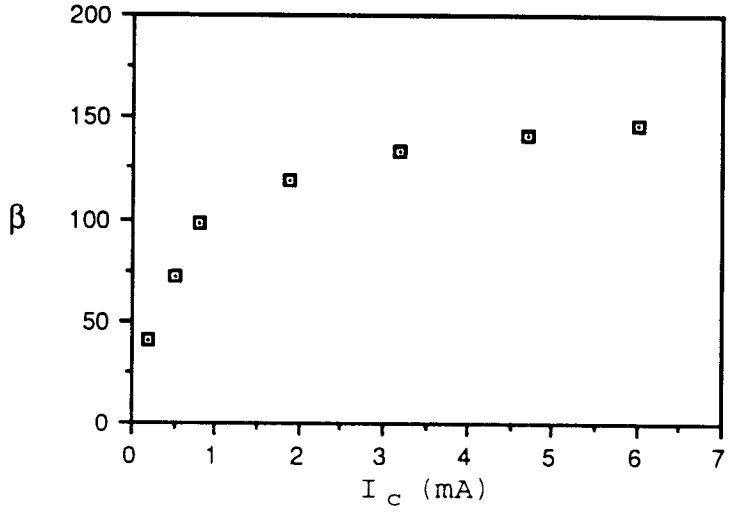

Figure 4.15. Current gain (β) versus collector current (I_c) for an HBT.

4.3.2.2. DX Centers in an HBT at Room Temperature

DLTS, DLAS, TSCAP, and C-V profiling analysis has established that DX is the only observable deep level in the emitter region of the AlGaAs/GaAs HBTs studied herein. However, there is a question of whether the DX center has any effect on the switching of HBTs at room temperature. The following discussion of this issue draws heavily on the work of Nathan *et al.* [90].

The existence of transient currents in AlGaAs/GaAs HBTs is discussed with the aid of Fig. 4.16. Figure 4.16(a) is an energy-band diagram for the HBT at zero bias. Since the AlGaAs is graded at both edges, no conduction band spikes are present. Most DX centers are filled with electrons except in the depletion region where they are empty. Figure 4.16(b) shows the emitter/base junction at forward bias; DX centers can capture electrons with a characteristic capture time given by

$$\tau_c = \frac{1}{\sigma V_{th} n} \tag{4.8}$$

where

$$\sigma = \sigma_\infty \exp\left(\frac{-E_{cap}}{KT}\right) . \tag{4.9}$$

At room temperature, τ_c = ~0.1 μsec. The transit time of electrons across the depletion region, τ_{scr}, is estimated as [89]

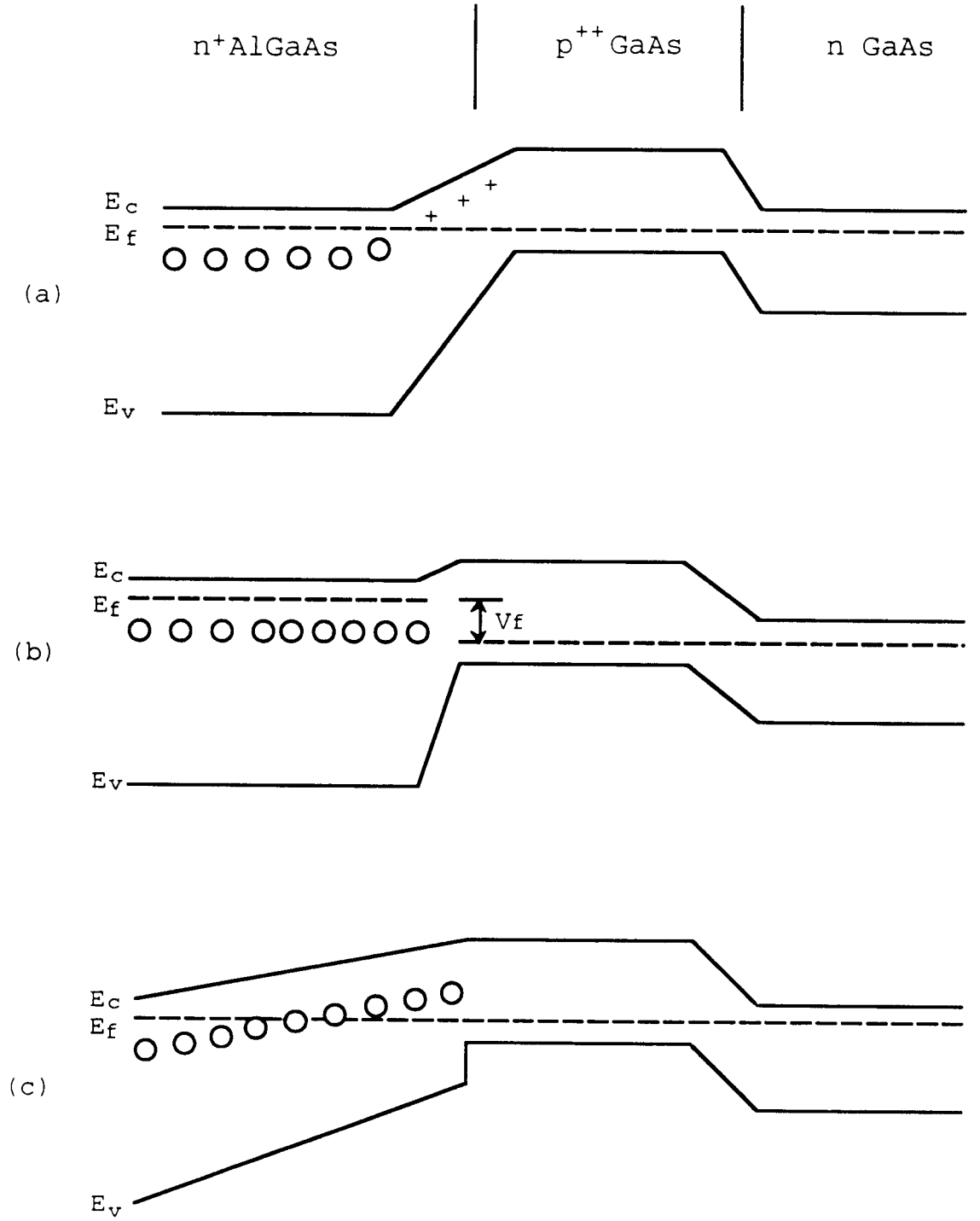

Figure 4.16. Approximate energy band diagrams for an HBT in which the emitter-base junction is operated under: (a) zero bias, (b) a large forward bias, and (c) at zero bias immediately following a application of a forward bias. The circles and plus signs represent neutral and ionized DX centers, respectively.

$$\tau_{scr} = \frac{(W_{scr})^2}{2D_n} \qquad (4.10)$$

where, D_n is the diffusion coefficient for an electron. From eqn. (4.10), τ_{scr} = ~10 psec. Thus, since $\tau_c >> \tau_{scr}$, very few electrons are expected to be captured in DX under forward bias and DX has a negligible effect on the turn-on transient of the HBT.

Now consider the situation shown in Fig. 4.16(c) in which some DX centers in the scr have been neutralized by a previously applied forward bias and then the bias is returned to zero bias. At room temperature, τ_e = ~0.1 sec (i.e., the DX emission time, as calculated from eqn. (3.2)), which is much larger than τ_{scr} = ~10 psec. DX emission in the scr also results in a transient current density, J, given by [90],

$$J = \frac{qN_tW_{scr}}{\tau_e} \; . \qquad (4\text{-}11)$$

For $N_t = 2.5\text{x}10^{17}$ cm^{-3}, W_{scr} = 700 Å, and τ_e = 0.1 sec, J = ~$2.8\text{x}10^{-6}$ A/cm^2 which is negligible compared to the current densities usually encountered in HBTs (~100 A/cm^2). Therefore, the presence of DX also has a very small effect on the turn-off characteristics of the HBT emitter/base junction.

Thus, although capture and emission of electrons at DX centers results in current transients when the HBT is

switched on or off, the magnitude of the current and thus its effect on the operation of an HBT is negligible.

At low temperature, the time for capture or emission of an electron from DX centers is slower than that at room temperature. Thus, at low temperature the switching characteristics of an HBT are also not affected by the presence of the DX center.

Chapter 5. Conclusions

In this thesis, deep level assessment of AlGaAs HBT emitters using DLTS, DLAS, TSCAP, and C-V profiling has been presented. DLTS was used to investigate the inter-dependences of two DX centers, DX_1 and DX_2, at different rate windows and filling pulse widths. The relationship between the DX center and the current gain as well as switching characteristics of HBTs has also been discussed.

The major conclusions of this experimental investigation are:

1. DX is the only deep level detected in the AlGaAs HBT emitter.

2. Two DX centers, DX_1 and DX_2, with activation energies of 0.40 and 0.44 eV, respectively, are observed in the HBT emitter layers. This is consistent with previous observations by other researchers [92].

3. The total DX concentration (i.e., the sum of DX_1 and DX_2) is about one half of the doping concentration; this is consistent with Chadi and Chang's negative U model for the DX center [55,56].

4. A positive peak observed in DLTS spectra is found to be an experimental artifact due to the small electron capture cross section of DX at low temperature (120 °K).

5. The 0.75 eV deep level commonly found in MBE grown AlGaAs layers is not observed. This is due to the high growth temperature of 630 °K used, which results in a substantial decrease in the concentration of this deep level [81]. Additionally, the presence of the 0.75 eV deep level is obscured by the relatively larger concentration of DX centers present in the HBT emitter layers.

6. At low collector current (I_C < 0.5 mA), DX center recombination dominates the current transport across the emitter/base and results in a low current gain (β) [89,94].

BIBLIOGRAPHY

[1] D. K. Schroder in *Semiconductor Material and Device Characterization* (John Wiley & Sons, Inc., New York, 1990).

[2] D. V. Lang, R. A. Logan, and M. Jaros, "Trapping Characteristics and a Donor-Complex (DX) Model for the Persistent-Photoconductivity Trapping Center in Te-doped $Al_xGa_{1-x}As$," Phys. Rev. B., Vol. 19, No. 2, p 1015-1030, 1979.

[3] M. G. Craford, G. E. Stillman, J. A. Rossi, and N. Holonyak, Jr., "Effect of Te and S Donor Levels on the Properties of $GaAs_{1-x}P_x$ near the Direct-Indirect Transition," Phys. Rev., Vol. 168, No. 3, p 867-882, 1968.

[4] D. V. Lang and R. A. Logan, "Chemical Shifts of DX Centers in $Al_xGa_{1-x}As$," Inst. Phys. Conf. Ser. No. 43, p 433-436, 1979.

[5] V. Narayanamurti, R. A. Logan, and M. A. Chin, "Symmetry of Donor-Related Centers Responsible for Persistent Photoconductivity in $Al_xGa_{1-x}As$," Phys. Rev. Lett., Vol. 43, No. 20, p 1536-1539, 1979.

[6] U.S. Patent No. 2,569,347, issued in 1951.

[7] H. Kroemer, Proc. IRE, vol. 45, "Theory of a Wide-Gap Emitter Transistors," p.1535-1537, 1957.

[8] Proc. IEEE, vol. 70, "Heterojunction Bipolar Transistors and Injected Circuits," p.13-25, 1982.

[9] A. Y. Cho, "Summary Abstract: Recent Developments in MBE and Summary of the MBE Conference in Japane, "J. Vac. Scien. Tech., vol. B1, No. 2, p.119-130, 1983.

[10] D. K. Jadus and D. L. Feucht, "The Realization of a GaAs-Ge Wide Band Gap Emitter Transistor, "IEEE Trans. Electron Dev., ED-16, p.102-107, 1969.

[11] H. J. Hovel and A. G. Milnes, "ZnSe-Ge Heterojunction Transistors," IEEE Trans. Electron Dev., ED-16, p.766-774, 1969.

[12] K.Sleger, A. G. Milnes, and D. L. Feucht, "A Technigue for fabricating Heterojunction Bipolar Transistors," Proc. Int. Conf. on Phys. and Chem. of Semiconductors, p.1-6, 1970.

[13] M. Konagai and K. Takahashi, "(GaAl)As-GaAs Heterojunction Transistors with High Injection Efficiency," J. Appl. Phys., vol. 46, p.2120-2124, 1975.

[14] M. Konagai and K. Katsukawa, and K. Takahashi, "(GaAl)As/GaAs Heterojunction Phototransistors with High Current Gain," J. Appl. Phys., vol. 48, p.4389-4394, 1977.

[15] J. S. Harris, P. M. Asbeck, and D. L. Miller, "High Speed HBTs for Microwave Applications," Proc. 14th Conf. on Solid State Devices, Tokyo, 1982 (Japn. J. Appl. Phys., vol.22, suppl., 22-1, p.375-377).

[16] D. Ankri, W. J. Schaff, P. Smith, and L. F. Eastman, "High-Speed GaAlAs-GaAs Heterojunction Bipolar Transistors with Near-Ballistic Operation," Electronics Lett., vol. 19, p.147-149, 1983.

[17] H. Ito, T. Ishibashi, and T. Sugeta, "High-Frequency Characteristics of AlGaAs/GaAs Heterojunction Bipolar Transistors," IEEE Electron Dev. Lett., EDL-5, p.214-216, 1984.

[18] P. M. Asbeck, D. L. Miller, R. J. Anderson, and F. H. Eisen, "GaAs/(Ga,Al)As Heterojunction Bipolar Transistors with Buried Oxygen-Implanted Isolation Layers," IEEE Electron Dev. Lett., EDL-5, p.310-312, 1984.

[19] P. M. Asbeck, D. L. Miller, and R. J. Anderson, "The Emitter Couple Logic Circuit using GaAs/(Ga,Al)As HBTs," Proc. GaAs Ic Symp., p.170-174, 1983.

[20] D. V. Lang in *Deep Centers in Semiconductors*, edited by S. T. Pantelides, (Gordon and Breach Science, New York, 1986) p 489-539.

[21] P. M. Mooney, "Deep Donor Levels (DX Centers) in III-V Semiconductors," J. Appl. Phys., Vol. 67, No. 3, p R1-R26, 1990.

[22] P. Bhattacharya, "The Relationship of the DX Center in $Al_xGa_{1-x}As$ and other III-V Alloys with the Conduction Band Structure," Semicond. Sci. Technol., Vol. 3, p 1145-1156, 1988.

[23] *Physics of DX Centers in GaAs Alloys*, edited by J. C. Bourgoin, Solid State Phenomena, Vol. 10, 1990.

[24] D. V. Lang and R. A. Logan, "Large-Lattice-Relaxation Model for Persistent Photoconductivity in Compound Semiconductors," Phys. Rev. Lett., Vol. 39, No. 10, p 635-639, 1977.

[25] H. Kunzel, A. Fischer, J. Knecht, and K. Ploog, "Investigation of Persistent Photoconductivity in Si-doped n-$Al_xGa_{1-x}As$ Grown by Molecular Beam Epitaxi," Appl. Phys. A., Vol. 32, p 69-78, 1983.

[26] R. J. Nelson, "Long-Lifetime Photoconductivity Effect in n-type GaAlAs," Appl. Phys. Lett., Vol. 31, No. 5, p 351-353, 1977.

[27] H. P. Hjalmarson and T. J. Drummond, "Deep donor Model for the Persistent Photoconductivity Effect," Appl. Phys. Lett., Vol. 48, No. 10, p 656-658, 1986.

[28] T. N. Theis and S. L. Wright, "Origin of "residual" Persistent Photoconductivity in Selectively Doped GaAs/$Al_xGa_{1-x}As$ Heterojunctions," Appl. Phys. Lett., Vol. 48, No. 20, p 1374-1376, 1986.

[29] N. Chand, R. Fischer, J. Klem, T. Henderson, P. Pearah, W. T. Masselink, Y. C. Chang, and H. Morkoc, "Beryllium and Silicon Doping Studies in $Al_xGa_{1-x}As$ and New Results on Persistent Photoconductivity," J. Vac. Sci. Technol. B. Vol. 3, No. 2, p 644-648, 1985.

[30] A. G. Milnes, "Semiconductor Heterojunction Topics: Introduction and Overview," Solid-State Electron., Vol. 29, No. 2, p 99-121, 1986.

[31] W. Timelthaler, W. Jantsch, and G. Weimann, "Persistent 2D Photoconductivity and Deep Levels in $Al_xGa_{1-x}As$/GaAs Heterostructures," Semicond. Sci. Technol., Vol. 5, p 686-690, 1990.

[32] P. M. Mooney, N. S. Caswell, and S. L. Wright, "The Capture Barrier of the DX center in Si-doped $Al_xGa_{1-x}As$," J. Appl. Phys., Vol. 62, No. 12, p 4786-4797, 1987.

[33] M. Tachikawa, M. Mizuta, and H. Kukimoto, "DX Deep Centers in $Al_xGa_{1-x}As$ Grown by Liquid-Phase Epitaxy," Jpn. J. Appl. Phys., Vol. 23, No. 12, p 1594-1597, 1984.

[34] P. M. Mooney, E. Calleja, S. L. Wright, and M. Heiblum, "Effect of the Host Band Structure on Capture and Emission Processes at DX Centers in AlGaAs," Materials Science Forum, Vol. 10-12, p 417-422, 1986.

[35] E. Calleja, A. Gomez, and E. Munoz, "Direct Evidence of the DX Center Link to the L-conduction-band Minimum in GaAlAs," Appl. Phys. Lett., Vol. 52, No. 5, p 383-385, 1988.

[36] N. Chand, T. Henderson, J. Klem, W.T. Masselink, and R. Fischer, "Comprehensive Analysis of Si-doped $Al_xGa_{1-x}As$(x=0 to 1): Theory and Experiments," Phys. Rev. B., Vol. 30, No. 8, p 4481-4492, 1984.

[37] E. F. Schubert and K. Ploog, "Shallow and Deep Donors in Direct-Gap n-type $Al_xGa_{1-x}As$:Si Grown by Molecular-Beam Epitaxy," Phys. Rev. B., Vol. 30, No. 12, p 7021-7029, 1984.

[38] T. Ishibashi, S. Tarucha, and H. Okamoto, "Si and Sn Doping in $Al_xGa_{1-x}As$ Grown by MBE," Jpn. J. Appl. Phys., Vol. 21, No. 8, p L476-L478, 1982.

[39] M. O. Watanabe, and H. Maeda, "Electron Activation Energy in Si-doped AlGaAs Grown by MBE," Jpn. J. Appl. Phys., Vol. 23, No. 9, p L734-L736, 1984.

[40] H. P. Hjalmarson and T. J. Drummond, "Long Lived Resonance States in Si-Doped AlGaAs," Materials Science Forum, Vol. 38-41, p 1091-1096, 1989.

[41] D. K. Maude, J. C. Portal, L. Dmowski, T. Foster, L. Eaves, M. Nathan, M. Heiblum, J. J. Harris, and R. B. Beall, "Investigation of the DX Center in Heavily Doped n-type GaAs," Phys. Rev. Lett., Vol. 59, No. 7, p 815-818, 1987.

[42] M. A. Fisher, A. R. Adams, E. P. O'Reilly, and J. J. Harris, "Resonant Electron Scattering due to the Central Cells of Impurities Observed in AlGaAs under Hydrostatic Pressure," Phys. Rev. Lett., Vol. 59, no. 20, p 2341-2344, 1987.

[43] T. N. Theis, P. M. Mooney, and S. L. Wright, "Electron Localization by a Metastable Donor Level in n-GaAs: A New Mechanism Limiting the Free-Carrier Density," Phys. Rev. Lett., Vol. 60, No. 4, p 361-364, 1988.

[44] A. K. Saxena, "The Conduction Band Structure and Deep Levels in $Ga_{1-x}Al_xAs$ Alloys from a High-pressure Experiment," J. Phys. C, Vol. 13, p 4323-4334, 1980.

[45] J. W. Matthews, A. E. Blakeslee, and S. Mader, "Use of Misfit Strain to Remove Dislocations from Epitaxial Thin Films," Thin Solid Films, Vol. 33, p 253-266, 1976.

[46] P. K. Bhattacharya, "Investigation of Persistent Photoconductivity in Si-doped n-$Al_xGa_{1-x}As$ Grown by Molecular Beam Epitaxi," Inst. Phys. Conf. Ser., vol. 45, p.199-203, 1979.

[47] A. K. Saxena, "Photoconductivity Storage in $Ga_{1-x}Al_xAs$ Alloys at Low Temperatures," Solid State Electron., Vol. 25, No. 2, p 127-131, 1982.

[48] M. O. Watanabe, K. Morizuka, M Mashita, Y. Ashizawa, and Y. Zohta, "Donor Levels in Si-doped AlGaAs Grown by MBE," Jpn. J. Appl. Phys., Vol. 23, No. 2, p L103-L105, 1984.

[49] M. F. Li, P. Y. Yu, E. R. Weber, and W. Hansen, "Photocapacitance Study of Pressure-Induced Deep Donors in GaAs:Si," Phys. Rev. B, vol. 36, p.4531-4534, 1987.

[50] M. F. Li, P. Y. Yu, E. R. Weber, and W. Hansen, "Lattice relaxation of Pressure-Induced Deep Centers in GaAs:Si," Appl. Phys. Lett., vol. 51, No. 5, p.349-351, 1987.

[51] D. K. Maude, J. C. Portal, L. Dmowski, T. Foster, L. Eaves, M. Nathan, M. Heiblum, J. J. Harris, and R. B. Beall, "Investigation of the DX Center in Heavily Doped n-type GaAs," Phys. Rev. Lett., Vol. 59, No. 7, p 815-818, 1987.

[52] J. C. M. Henning and J. P. M. Ansems," A New Model of Deep Donor Centers in $Al_xGa_{1-x}As$, "Materials Science Forum, Vol. 10-12, p 429-434, 1986.

[53] J. C. M. Henning and J. P. M. Ansems, "A New Model of Deep Donor Centers in $Al_xGa_{1-x}As$," Semicond. Sci. Technol., Vol. 2, p 1-13, 1987.

[54] P. M. Mooney, G.A. Northrop, T. N. Morgan, and H. G. Grimmeiss, "Evidence for Large Lattice Relaxation at the DX Center in Si-doped $Al_xGa_{1-x}As$," Phys. Rev. B., Vol. 37, No. 14, p 8298-8307, 1988.

[55] D. J. Chadi and K. J. Chang, "Theory of the Atomic and Electronic Structure of DX Centers in GaAs and $Al_xGa_{1-x}As$ Alloys," Phys. Rev. Lett., Vol. 61, No. 7, p 873-876, 1988.

[56] D. J. Chadi and K. J. Chang, "Energetic of DX-Center Formation in GaAs and $Al_xGa_{1-x}As$ Alloys," Phys. Rev. B., Vol. 39, No. 14, p 10063-10074, 1989.

[57] P. W. Anderson, "A Model for the Electronic Structure of Amorphous Semiconductors," Phys. Rev. Lett., vol. 34, No. 15, p.953-955, 1975.

[58] O. Kumagai, H. Kawai, Y. Mori, and K. Kaneko, "Chemical Trends in the Activation Energies of DX centers," Appl. Phys. Lett., vol. 45, No. 12, p.1322-1325, 1984.

[59] Defects in Semiconductors, edited by G. Ferenczi, "Lattice relaxation of Pressure-Induced Deep Centers in GaAs:Si," (Trans. Tech., Switzland,1989), p.1067-1070, 1989.

[60] K. A. Khachaturyan, D. D. Awschalom, J. R. Rozen, and E. R. Weber, "Magnetic Studies of Persistent Photoconductivity in n-AlxGa1-xAs," Phys. Rev. Lett., vol. 63, p.1311-1314,1989.

[61] D. V. Lang, "Deep-level Transient Spectroscopy: A New Method to Characterize Traps in Semiconductors," J. Appl. Phys., Vol. 45, No. 7, p 3023-3032, 1974.

[62] G. L. Miller, D. V. Lang, and L. C. Kimerling, "Capacitance Transient Spectroscopy," Ann. Rev. Mater. Sci. p 377-448, 1977.

[63] D. L. Losee, "Admittance Spectroscopy of Impurity Levels in Schottky Barriers," J. Appl. Phys., Vol. 46, No. 5, p 2204-2214, 1975.

[64] J. C. Carballes and J. Lebailly, "Trapping Analysis in Gallium Arsenide," Solid State Commun., vol. 6, p.167-171, 1968.

[65] L. R. Weisberg and H. Schade, "A Technique for Trap Determination in Low-Resistivity Semiconductor," J. Appl. Phys., vol. 39. p.5149-5151, 1968.

[66] R. Decker, "Measurement of Epitaxial Doping Density vs. Depth," J. Elecro. Chem. Soc., vol. 115, p.1085-1089, 1968.

[67] L. E. Coever, "Note on the Intepretation of C-V Data in Semiconductor Junctions," IEEE Trans. Electron Dev., ED-17, p.436, 1970.

[68] H. J. J. DeMa, "On the Calculation of Doping Profiles from C(V) Measurements on Two-Sided Junctions," IEEE Trans. Electron Dev., ED-17, p.1087-1088, 1970.

[69] M. Nathan, P. M. Mooney, P. M. Solomon, and S. L. Wright, "Room-Temperature Electron Trapping in $Al_{0.35}Ga_{0.65}As$/GaAs Modulation-Doped Field-Effect Transistors," Appl. Phys. Lett., Vol. 47, No. 6, p 628-630, 1985.

[70] R. Fischer, T. J. Drummond, J. Klem, W. Kopp, T. S. Henderson, D. Perrachione, and H. Morkoc, "On the Collapse of Drain I-V Characteristics in Modulation-Doped Fet's at Cryogenic Temperatures," IEEE Trans. Electron Dev., ED-33, p.1028-1032, 1984.

[71] A. Thomasian, N. L. Saunders, L. G. Hipwood, and A. A. Rezazadeh, "Mechanism of Kink Effect Related to Negative Photoconductivity in AlGaAs/GaAs HEMTs," Electronic Letters, Vol. 25, No. 11, p 738-739, 1989.

[72] S. J. Prasad, B. Vetanen, C. Haynes, S. Park, I. Beers, S. Diamond, G. Pubanz, J. Ebner, S. Sanielevici, and A. Agoston, "An Implant-Free AlGaAs/GaAs HBT IC Technology Incorporating 1.4 THz Schottky Diodes," IEEE 1991 Bipolar Circuits and Technology Meeting, p.79-82, 1991.

[73] M. O. Watanabe, K. Morizuka, M Mashita, Y. Ashizawa, and Y. Zohta, "Donor Levels in Si-doped AlGaAs Grown by MBE," Jpn. J. Appl. Phys., Vol. 23, No. 2, p L103-L105, 1984.

[74] J. R. Hayes, F. Capasso, R. J. Malik, A. C. Gossard, and W. Weigmann, "Elimination of the Emitter/Collector Offset Voltage in Heterojunction Bipolar Transistor," IEEE Int. Electron Devices Meeting Technical Digest, p.686, 1983.

[75] D. G. Deppe, "Thermodynamic Explanation to the Enhanced Diffusion of Base Dopant in AlGaAs-GaAs npn Bipolar Transistor," Appl. Phys. Lett., vol. 56, p.370-372, 1990.

[76] P. Enquist, L. M. Lunardi, D. F. Welch, G. W. Wicks, J. R. Shealy, L. F. Eastman, and A. R. Calawa, "Optimization of the Injection Efficiency (γ) of the HBT by Studying Eluminescence (EL) of MBE Heterojunction Diodes," Inst. Phys. Conf. Ser., No. 74, p.599-604, 1984.

[77] A. Baldereschi, "Valley-Orbit Interaction in Semiconductor," Phys. Rev. B, vol. 1, No. 12, p.4673-4677, 1970.

[78] K. Shindo and H. Nara, "The Efffective Mass Equation for the Multi-Valley Semiconductors," J. Phys. Soc. Japn., vol. 40, No. 6, p.1640-1644, 1976.

[79] M. Mizuta, M. Tachikawa, H. Kukimoto, and S. Minomura, "Direct Evidence for the DX Center Being a Substitutional Donor in AlGaAs Alloy System," Jpn. J. Appl. Phys., Vol. 24, No. 2, p L143-L146, 1985.

[80] J. H. Reuszer and P. Fisher, "An Optical Determination of the Ground-State Spliting of Group V Impurities in Germanium," Phys. Rev., vol. 135, No. 4A, p.A1125-A1132, 1964.

[81] P. M. Mooney, R. Fischer, and H. Morkoc, "Transient Capacitance Study of Electron Traps in AlGaAs Grown with As_2," J. Appl. Phys., Vol. 57, No. 6, p 1928-1931, 1985.

[82] K. Yamanaka, S. Naritsuka, M. Mannoh, T, Yuasa, Y. Nomura, M. Mihara, and M. Ishii, "Influence of Growth Conditions and Alloy Composition on Deep Electron Traps of n-AlxGa1-xAs Grown by MBE," J. Vac. Sci. Technol., B2, p.229-232, 1984.

[83] N. Tsukada, T. Kikuta, and K. Ishida, "Photo-Electron Paramagnetic Resonance Study of As_{Ga} Antisite Defect in As-Grown GaAs Crystala of Different Stoichiometry," Japn. J. Appl. Phys., vol. 24, P.L689-L692, 1985.

[84] M. Kaminska, M. Skowronski, and W. Kuszko, "Identification of the 0.82-eV Electron Trap, EL2, in GaAs, as an Isolated Antisite Arsenic Defect," Phys. Rev. Lett., vol. 55, No. 20, p.2204-2207, 1985.

[85] J. J. Lagavski, H. C. Gatos, J. M. Parsey, K. Wada, M. Kaminska, and W. Walukiewicz, "Origin of the 0.82-eV Electron Trap in GaAs and its Annihilation by Shallow Donors," Appl. Phys. Lett., vol. 40, p.342-344, 1982.

[86] J. A. Van Vechten, "Thermodynamics of Deep Levels in Semiconductors," Mat. Res. Soc. Symp. Proc., Vol. 46, p 83-103, 1985.

[87] H. J. Von Bardeleben, D. Stievenard, J. C. Bourgoin, and A. Huber, "Identification of EL2 in GaAs," Appl. Phys. Lett., vol. 47, No. 9, p.970-972, 1985.

[88] G. M. Martin, E. Esteve, P. Langlade, and S. Markram_Ebeid, "Kinetics of Formation of the Midgap Donor EL2 in Neutron Irradiated GaAs Materials," J. Appl. Phys., vol. 56, p.2655-2657, 1984.

[89] S. M. Sze in *Physics of the Semiconductor Devices* (John Wiley & Sons, Inc., New York, 1981).

[90] M. I. Nathan, S. Tiwari, P. M. Mooney, and L. Wright, "DX centers in AlGaAs p-n Heterojunction and Heterojunction Bipolar Transistors," J. Appl. Phys., vol. 62, p.3234-3236, 1987.

[91] E. Calleja, A. Gomez, E. Munoz, and P. Camara, "Fine Structure of the alloy-broadened thermal emission spectra from DX centers in GaAlAs," Appl. Phys. Lett., vol. 52, No. 22, p.1877-1879, 1988.

[92] P. M. Mooney, T. N. Theis, and S. L. Wright, "Effect of local alloy disorder on emission kinetics of deep donors (DX centers) in AlGaAs of Low Al Content," Appl. Phys. Lett., vol. 53, No. 25, p.2546-2548, 1988.

[93] P. Basmaji, M. Guittard, and P. Gibart, "Enhancement of the Free Carrier Density in Ga AlAs Grown by Metallorganic Vapor Phase Epitaxy under High Temperature Growth Conditions," Phys. Status Solidi (a), vol. 100, p.K41-K45, 1987.

[94] A. A. Rezazadeh, J. A. Barnard, and T. M. Kerr, "The Role of Electron Traps in the d.c. Current Gain of GaAs/GaAlAs Heterojunction Bipolar Transistors Prepared by MBE," Inst. Phys. Conf. Ser., No. 79, p.601-606, 1985.